Title: Lipidomic and biophysical homeostasis of mammalian membranes in response to dietary lipids is essential for cellular fitness

Short title: Physical homeostasis of mammalian membranes

Authors: Kandice R Levental*, Eric Malmberg, Jessica Symons, Yang-Yi Fan, Robert S. Chapkin, Robert Ernst, Ilya Levental*

Authors affiliations: Kandice R Levental[a], Eric Malmberg[a], Jessica Symons[a], Yang-Yi Fan[b], Robert S. Chapkin[b], Robert Ernst[c], Ilya Levental[a]

[a]University of Texas Health Science Center at Houston, Houston, TX, USA

[b]Program in Integrative Nutrition & Complex Diseases and Department of Nutrition & Food Science, Texas A&M University, College Station, TX, USA.

[c]Department of Medical Biochemistry and Molecular Biology, Medical Faculty, Saarland University, 66421 Homburg, Germany

***Co-corresponding authors:** Dr. Ilya Levental and Dr. Kandice Levental

Address: Suite 4.202A, 6431 Fannin St, Houston, TX, USA 77030

Phone: +1–713–500–5566

Fax: +1–713–500–7456

Email: ilya.levental@uth.tmc.edu ; kandice.r.levental@uth.tmc.edu

Keywords: membrane fluidity, lipidomics, diet, homeostasis, adaptation, saturated, polyunsaturated, fatty acid, cholesterol, SREBP

ABSTRACT

Biological membranes form the functional, dynamic interface that hosts a major fraction of all cellular bioactivity. Proper membrane physiology requires maintenance of a narrow range of physicochemical properties, which must be buffered from external perturbations. While homeostatic adaptation of membrane fluidity to temperature variation is a ubiquitous design feature of ectothermic organisms, such responsive membrane adaptation to external inputs has not been directly observed in mammals. Here, we report that challenging mammalian membrane homeostasis by dietary lipids leads to robust lipidomic remodeling to preserve membrane physical properties. Specifically, exogenous polyunsaturated fatty acids (PUFAs) are rapidly and extensively incorporated into membrane lipids, inducing a reduction in membrane packing. These effects are rapidly compensated both in culture and *in vivo* by lipidome-wide remodeling, most notably upregulation of saturated lipids and cholesterol. These lipidomic changes result in recovery of membrane packing and permeability. This lipidomic and biophysical compensation is mediated in part by lipid regulatory machinery, whose pharmacological or genetic abrogation results in cytotoxicity when membrane homeostasis is challenged by dietary lipids. These results reveal an essential mammalian mechanism for membrane homeostasis wherein lipidome remodeling in response to dietary lipid inputs preserves functional membrane phenotypes.

INTRODUCTION

Lipidic membranes are the essential barriers between life and the abiotic world and also mediate most intracellular compartmentalization in eukaryotic cells. However, the functions of membranes are not limited to passive barriers. Approximately one third of all proteins are membrane-embedded [1], and many more are membrane-associated through post-translational modifications, lipid binding, and protein-protein interactions. Thus, a major fraction of cellular bioactivity occurs at membrane interfaces. Importantly, the physicochemical properties of the lipid matrix are key contributors to membrane physiology. A canonical example is membrane viscosity, which determines protein diffusivity, and thus protein-protein interaction frequency. Another is membrane permeability, which governs the diffusion of solutes into and out of the cytosol. Numerous other membrane physical parameters can determine protein behavior, including but not limited to fluidity, permeability, curvature, tension, packing, bilayer thickness, and lateral compartmentalization [2-12].

Because of their central role in protein function, effective maintenance of membrane properties is essential for cell survival in complex and variable environments. In ectothermic (i.e. non-thermoregulating)

organisms, a pervasive challenge to membrane homeostasis comes from temperature variations. Low temperature reduces the motion of lipid acyl chains, causing membranes to laterally contract, stiffen, and become more viscous [13]. Organisms across the tree of life, from prokaryotes to ectothermic animals, respond to such perturbations by tuning membrane lipid composition, down-regulating tightly packing lipids (e.g. containing saturated acyl chains) and up-regulating more loosely packed ones containing unsaturations or methylations in their lipid tails [13-15]. This response was termed 'homeoviscous adaptation', as these lipid changes result in remarkable constancy in membrane fluidity in spite of variable growth conditions [13,14,16]. It is worth noting that while fluidity is maintained at a specific set point, it should not be assumed that it is either the control variable or the physical property being sensed; rather membrane fluidity may correlate with other membrane/lipid control parameters. For example, membrane homeostasis in *Bacillus subtilis* is mediated by the DesK sensor that is believed to sense membrane thickness [17]. In the yeast endoplasmic reticulum (ER), recently discovered sensors are sensitive specifically to lipid packing [5] and bilayer compressibility [18].

Excepting a few specialized instances (e.g. hibernation), mammals and other warm-blooded animals are not subject to large-scale variations in body temperature; thus, there has been relatively little investigation of homeostatic membrane responsiveness in such organisms. However, it is a well-established but under-appreciated fact that mammalian membrane homeostasis is extensively challenged by dietary inputs. Dietary lipids have major impacts on membrane compositions *in vivo* [19,20], and these perturbations must presumably be buffered to maintain cellular functionality. Mammalian lipidomes are much more complex [21-23] than either bacteria [24] or yeast [25,26], suggesting more potential control nodes required to balance the various conflicting demands of mammalian membrane physiology.

The possibility of a homeoviscous response in mammalian cells was suggested by two studies in the 1970s, which used a spontaneously arising mutant of Chinese Hamster Ovary (CHO) cells that is defective in cholesterol regulation [27,28]. These mutants accumulate cholesterol compared to wild-type CHO cells, but maintain normal membrane fluidity, possibly through modulation of their phospholipid profiles. However, the molecular etiology of the defects in these mutants remains unknown, and it was not reported where the cholesterol in these cells was accumulating (possibly storage organelles or lysosomes). Further, limitations of then-available technologies prevented direct demonstration of lipidomic responses to cholesterol modulation. Thus, the relevance of those insights to physiologically relevant perturbations of metabolically normal mammalian cells remains unclear. More recently, homeoviscous adaptation in mammals has been inferred from data-driven modeling approaches, which used the physical properties (melting temperature, intrinsic curvature) of pure lipids to extrapolate those of complex, biological

87 membranes [29,30]. However, the inherent non-additivity [31] and non-ideality [32] of lipid mixtures suggests that
88 extrapolation of physical parameters of complex membranes from pure lipids may not be a reliable
89 approach. Finally, lipid composition and membrane properties have been implicated in the heat shock
90 response, though usually with a specific focus on signaling of the proteostasis network [33].

91 Here, we directly evaluate the hypothesis that mammalian membranes homeostatically adapt to dietary
92 inputs by characterizing the lipidomic and biophysical responses to dietary fatty acids in cultured
93 mammalian cells and *in vivo*. Using shotgun mass spectrometry, we show that polyunsaturated fatty acids
94 (PUFAs) are robustly incorporated into membrane phospholipids, introducing significant biophysical
95 perturbations. This perturbation is counterbalanced by rapid lipidomic remodeling, most notable in the
96 upregulation of saturated lipids and cholesterol. This remodeling normalizes membrane permeability and
97 lipid packing, as evaluated by spectral imaging of the solvatochromic dye C-Laurdan. These responses
98 are mediated in part by transcriptional sterol-regulatory machinery involving the Sterol Regulatory
99 Element Binding Protein 2 (SREBP2), whose genetic or pharmacological inhibition abrogated lipidomic
100 and biophysical homeostasis. Finally, we show that the homeostatic membrane response is essential for
101 cellular fitness, as un-compensated lipidomic perturbations lead to increased membrane permeability and
102 non-apoptotic cell death when membrane homeostasis is challenged by exogenous fatty acids.

103

104 **RESULTS**

105 *Robust incorporation of PUFAs into membrane lipids*

106 Recent observations revealed that supplementation of cultured mammalian mast cells (rat basophilic
107 leukemia cells (RBL)) with docosahexaenoic acid (DHA) leads to robust incorporation of this dietary
108 polyunsaturated fatty acid into membrane lipids [23]. We observed similar effects in isolated human
109 mesenchymal stem cells [34], cultured Chinese hamster ovary (CHO) cells, and rat primary hippocampal
110 neurons (Supp Fig S1), confirming that uptake and incorporation of exogenous DHA into membrane lipids
111 is not cell-type specific. Supplementation designed to recapitulate DHA-enriched diets in mammals (see
112 Materials and Methods) increased the fraction of DHA-containing glycerophospholipids (GPLs) by nearly
113 15-fold (from <1 to ~15 mol%) (Fig 1A). Similarly, supplementation with the more common PUFA ω-6
114 arachidonic acid (AA) increased the fraction of AA-containing lipids by >3-fold (Fig 1B). Surprisingly,
115 supplementation with monounsaturated (oleic; OA) acid or saturated (palmitic; PA) fatty acid produced
116 only minimal lipidomic changes (Supp Fig S2). We expect that this disparity in incorporation is associated
117 with the availability of these fatty acids in cell culture media[35]: cultured cells have access to sufficient

118 OA and PA such that supplementation at concentrations used here has no effect, whereas PUFA levels are
119 limited such that supplementation with the physiologically appropriate concentrations used here leads to
120 robust uptake and incorporation.

121 To confirm that the membrane incorporation of supplemented PUFAs in cultured cells appropriately
122 recapitulates *in vivo* conditions, we analyzed membrane lipidomes in mouse cardiac tissue after two weeks
123 of *ad libitum*-feeding on a semi-purified diet containing either fish oil (FO) or corn oil (CO), as previously
124 described [36]. The FO diet is highly enriched in long-chain PUFAs, with ω-3 DHA and eicosapentaenoic
125 acid (EPA; 20:5) comprising ~20% of all fatty acids. In contrast, CO is poor in long-chain PUFAs (1.3%
126 FAs with 3+ unsaturations), with ω-6 linoleic acid (18:2) being the major PUFA source (>50% of dietary
127 FAs) (see Supplement Table 1 for full dietary lipid profile). Consistent with previous observations[36-38] and
128 the *in vitro* measurements here, dietary fish oil supplementation produced a robust incorporation of ω-3
129 PUFAs into cardiac membrane lipids, with ~18-fold more ω-3 PUFA-containing membrane lipids in the
130 FO-fed compared to CO-fed tissues (Fig 1D). As a result, FO-fed mice had a significantly higher
131 proportion of lipids containing long, highly unsaturated acyl chains (5 or 6 double bonds; Fig 1E), which
132 resulted in an overall increase in unsaturation of FO-fed tissues (Fig 1F).

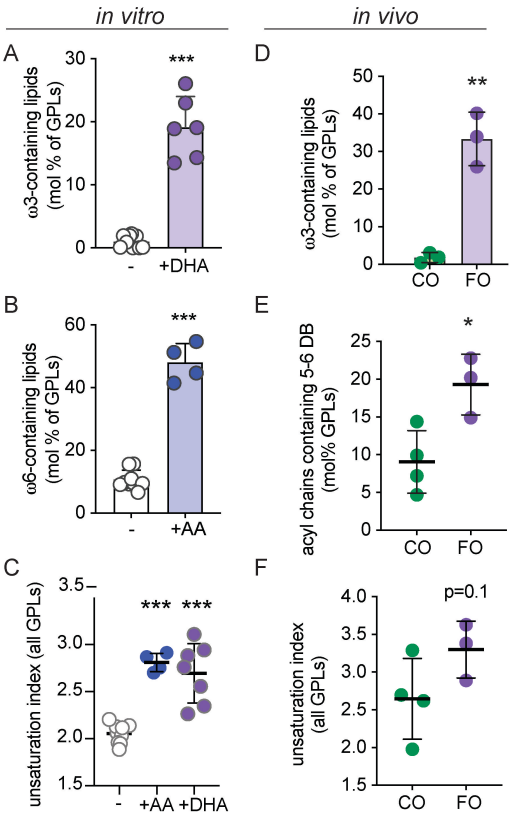

133

134 **Fig 1. Supplemented PUFAs are robustly incorporated into membrane phospholipids *in vitro* and *in vivo*.**
135 Supplementation of culture media with PUFAs for 3 days (20 μM) leads to a dramatic increase in (A) ω–3 PUFA-containing
136 membrane lipids in RBL cells supplemented with DHA and (B) ω–6 PUFA-containing membrane lipids supplemented with AA.
137 (C) Both treatments result in significantly increased overall unsaturation of membrane lipids. The unsaturation index reflects a
138 concentration-weighted average lipid unsaturation. (D) Mice fed a diet rich in fish oil (FO) have significantly more lipids containing
139 ω–3 PUFAs compared to corn oil (CO) fed mice. (E) Incorporation of dietary ω–3 PUFAs increases cardiac tissue lipids
140 containing very highly unsaturated (5 or 6 double bonds) acyl chains, resulting in an (F) increase in the overall unsaturation of
141 membrane glycerophospholipids. Individual experiments (A-C) or animals (D-F) are shown. Bars represent mean ± SD.
142 **p<0.01, ***p<0.001 for unpaired t-test compared to untreated. Treatment with saturated (PA) or monounsaturated (OA) fatty
143 acids in these conditions had no effect on the lipidome (see Fig S2).

144

145 *Lipidome remodeling associated with PUFA incorporation*

146 Despite the copious incorporation of exogenous PUFAs into membrane lipids and the resulting increase
147 in overall membrane unsaturation (Fig 1), cells *in vitro* did not show any obvious toxicity or differences
148 in proliferation at these levels of supplementation (Fig S3). This observation was somewhat surprising in
149 light of the central role of lipid unsaturation in membrane physical properties [39,40] and the putatively
150 critical role of those properties in regulating various cellular processes [3,4,7]. Thus, we hypothesized that
151 mammalian cells may compensate for perturbations from exogenous FAs by remodeling their lipidomes.
152 Indeed, while treatments with OA/PA had no effect on overall cell lipidomes (Supp Fig S2; consistent
153 with their lack of incorporation), both AA and DHA supplementation reduced the abundance of other
154 polyunsaturated (i.e. di- and tri-unsaturated) lipid species (Fig 2A-B). This effect could potentially be
155 explained by replacement of these PUFA-containing lipids by AA/DHA-containing ones. Much more
156 surprising was the highly significant increase in fully saturated lipids resulting from PUFA
157 supplementation (Fig 2A), due to the significantly increased abundance of phospholipid-incorporated
158 saturated fatty acids (Fig 2A inset). This analysis reveals approximately 2-fold more fully saturated lipids
159 resulting from DHA and AA supplementation, respectively (Fig 2A). These changes were associated with
160 a significantly reduced overall unsaturation in phospholipids not containing the supplemented FAs (Fig
161 2B-C, see figure legend for details). These effects were, at least in part, transcriptionally mediated, as
162 evidenced by mRNA levels of the major fatty acid desaturase enzymes SCD1 and SCD2. As previously
163 reported [41], both were substantially down-regulated by DHA treatment (Fig S4), consistent with more
164 saturated and fewer polyunsaturated lipids. The headgroup profile of membrane lipids was not notably
165 affected by any of the treatments (Supp Fig S5).

166 This lipidomic remodeling in response to PUFA feeding *in vitro* was not limited to a single cell type. The
167 observations described so far were on a transformed leukocyte cell line (RBL); however, very similar
168 DHA-induced lipid changes were observed in cultured CHO cells, primary rat hippocampal neurons,
169 primary human MSCs, and MSCs that were differentiated *in vitro* into osteoblasts or adipocytes (Fig. 2D).
170 Not only the broad trends of the lipidomic remodeling (more saturated, less unsaturated lipids) were
171 common between these disparate cell lineages and sources, but also the magnitude of the effects were
172 quantitatively similar, despite drastic differences in overall lipid composition [23,34,42,43]. The similarity of
173 the responses between freshly isolated cells, cultured primary cells, and long-term cultured cells lines
174 derived from two different germ layers and three different organisms suggests that comprehensive
175 lipidomic remodeling in response to exogenous PUFAs is a general phenomenon for mammalian cells.

176 Importantly, this response is also evident *in vivo*. The incorporation of highly polyunsaturated PUFAs
177 from the diet into membrane lipids in mouse cardiac tissue (Fig 1D-E) led to remarkably similar lipidomic
178 remodeling as was observed in cultured cells. Namely, we observed that FO fed-mice have ~2-fold more
179 saturated lipids compared to CO-fed mice, consistent with compensatory, homeostatic lipidomic
180 remodeling *in vivo* (Fig 2E). The striking differences between FO and CO feeding are notable in light of
181 the fact that CO diets do contain abundant PUFAs in the form of linoleic acid (18:2). These differences
182 are potentially due to the unique effects of highly polyunsaturated lipids on membrane properties, which
183 scale with the degree of unsaturation[43,44]. An alternative, non-exclusive possibility is that highly
184 unsaturated FAs are preferentially taken up into membrane lipids. These details will be resolved by future
185 studies with various FA feeding protocols.

186

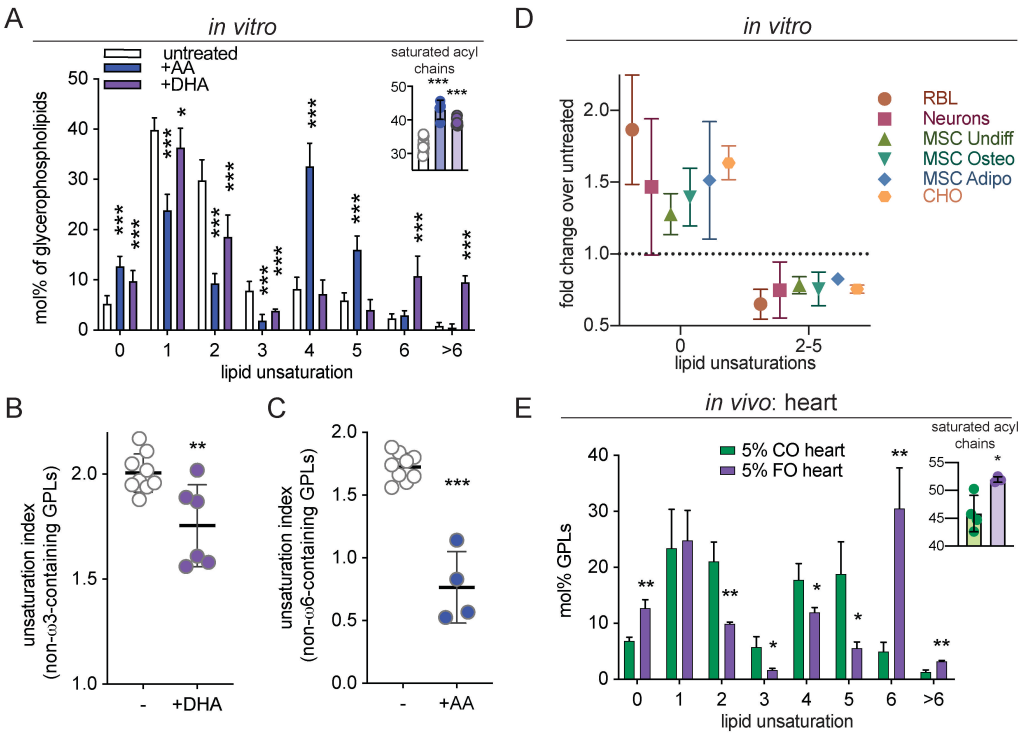

Figure 2 – Lipidome remodeling induced by PUFA incorporation. (A) Lipidome-wide remodeling of lipid unsaturation induced by DHA or AA supplementation. Both PUFAs induce significantly increased saturated lipids and decrease lipids containing di- and tri-unsaturated lipids. Inset shows the mol% of fully saturated acyl chains in GPLs. (B and C) The unsaturation index (concentration-weighted average lipid unsaturation) of lipids not containing the supplemented FAs and their derivatives is significantly reduced upon PUFA supplementation. For accurate estimates of lipidomic remodeling, the supplemented FAs and their derivatives are removed from the analysis, as the rather extreme over-abundance of those species upon supplementation suppresses the visualization of compensatory effects (e.g. for DHA supplementation, lipids containing 22:6, 20:5, or 24:6 are removed and then the unsaturation index of the "remaining" lipids is calculated). (D) DHA-mediated lipidomic remodeling, indicated by increased saturated lipids and decreased polyunsaturated lipids (2-5 unsaturations), is consistent across multiple cell types, including isolated rat hippocampal neurons, cultured human MSCs, and MSC differentiated into adipogenic or osteogenic lineages. (E) Lipid unsaturation profile in membrane lipids isolated from murine heart tissue after feeding with CO versus FO. Incorporation of ω-3 PUFAs into membrane lipids (see Fig 1D) is associated with other lipidomic remodeling, namely higher levels of saturated lipids. Inset shows the mol% of fully saturated acyl chains in GPLs. All data are average +/- SD for n ≥ 3 biological replicates. A and E are two-way ANOVA with Sidak's multiple comparison test. B-C and insets are student's t-test compared to untreated. *p<0.05, **p<0.01, ***p<0.001.

Lipidomic remodeling is nearly concomitant with exogenous PUFA incorporation

The remodeling associated with PUFA incorporation into membrane lipids suggested the induction of a homeostatic membrane response, wherein saturated lipids are upregulated to compensate for the fluidizing effect of PUFA-containing species. To support this inference, we analyzed the temporal profiles of PUFA

208 incorporation and associated lipidomic changes *in vitro*. DHA was quickly incorporated into membrane
209 lipids, with significant increases in DHA-containing lipids observed within 1 h of supplementation and
210 half-time of incorporation of ~4 h (Fig 3A-B). The recovery time course was significantly slower, as wash-
211 out of DHA was followed by a return to baseline with a half-time of ~25 h (Fig 3C). This is the
212 approximate doubling time of RBL cells in culture, suggesting that the "wash-out" effect likely results
213 from dilution by new lipid synthesis rather than directed removal of DHA from membrane lipids.
214 Remarkably, the associated lipidome remodeling proceeded with similar temporal profiles to both DHA
215 supplementation and wash-out (Fig 3D-I). The increase in saturated lipids (Fig 3E) and the decrease in di-
216 unsaturated lipids (Fig 3H) were observed shortly after DHA incorporation and similar time courses were
217 also observed for the wash-out (Fig 3F and 3I). These observations reveal unexpectedly abrupt lipidomic
218 perturbations and suggest that such perturbations induce rapid compensatory responses.

219 The broad compensatory lipidomic remodeling in response to PUFA supplementation in mammalian cells
220 evokes comparisons to classical observations of homeoviscous adaptation in ectothermic (i.e. non-
221 thermoregulating) organisms [13-16,45,46]. There, perturbations of membrane physical properties produced by
222 changes in ambient temperature induce lipid changes whose apparent purpose is to re-normalize
223 membrane physical properties. Our findings suggest that a similar response to fluidizing stimuli occurs in
224 mammalian cells, where it has been co-opted to cope with perturbations from exogenous lipids (e.g. from
225 the diet).

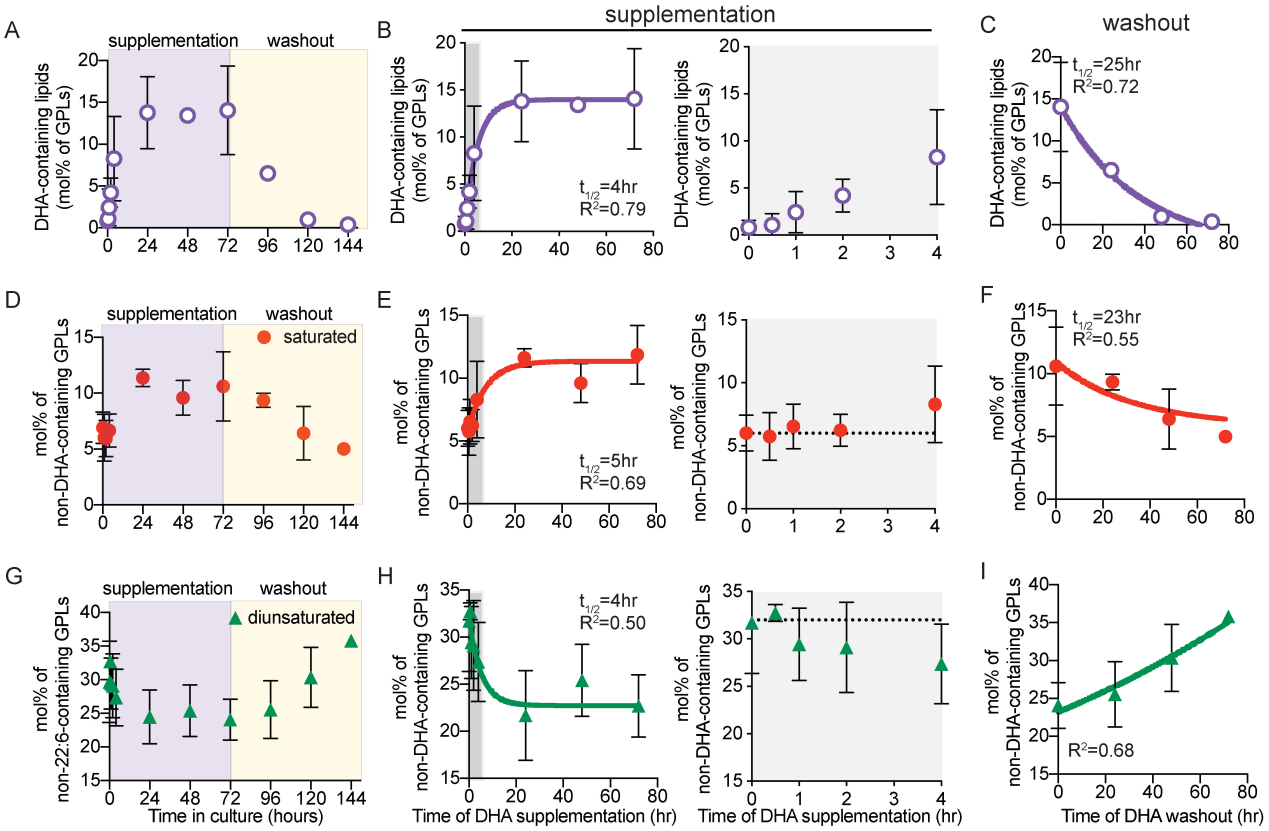

Figure 3 – Time course of DHA incorporation and lipidome remodeling. (A-C) Time course of DHA incorporation into GPLs following supplementation, then wash-out. Time course of nearly concomitant (D-F) saturated lipid and (G-I) di-unsaturated lipid changes induced by DHA supplementation. The gray areas in B, E, and H are shown in extended charts to the right of each panel to illustrate the timing of the remodeling. All data shown are average +/- SD for n ≥ 3 biological replicates. All fits shown are first-order kinetic models.

Cholesterol upregulation by DHA via SREBP2

The above-described acyl chain remodeling in response to PUFA supplementation was incomplete, as the unsaturation index of PUFA-supplemented cells remained higher than those from untreated controls (Fig 1C and 1F). If the purpose of this lipidome response is to normalize membrane properties, the acyl chain remodeling appears insufficient on its own (lipid headgroup remodeling was minimal; Fig S5C). In contrast to most prokaryotes wherein membrane homeostasis is mediated largely by phospholipids [14], membrane properties in eukaryotes are regulated to a very significant extent by sterols [47,48]. Thus, we hypothesized that the adaptive response to PUFA perturbation in mammalian cells was also mediated by cholesterol. Indeed, DHA supplementation led to significantly increased membrane cholesterol in both FO-fed murine heart tissue (Fig 4A) and cultured cells (Fig 4B). In cells, the increase in cholesterol

243 abundance was again quite rapid, with effects observed within 1 h of DHA introduction and reaching a
244 peak after ~4 h (Fig 4C), essentially concomitant with the acyl chain remodeling (Fig 3). There was also
245 evidence of a small but notable overshoot, as the cholesterol increase was somewhat attenuated after ~4
246 hrs. These observations suggest that cholesterol upregulation is an early and potent response to membrane
247 perturbation.

248 The machinery for cholesterol production in metazoans is regulated by proteolytic processing of
249 transcription factors of the sterol regulatory element binding protein (SREBP) family [49]. Specifically,
250 signals to upregulate cellular cholesterol levels are translated into proteolysis of a membrane-bound
251 SREBP2 precursor to release a 'mature' cleaved fragment, which translocates to the nucleus to induce
252 transcription of various target genes, including those for cholesterol synthesis and uptake [49]. Having
253 observed a robust and rapid increase in cholesterol levels resulting from DHA supplementation, we
254 evaluated whether SREBP2 processing was associated with this response. Indeed, DHA feeding increased
255 the production of the 'mature' transcription factor form of SREBP2, with minimal effect on the precursor
256 form (Fig 4D and Supp Fig S6). In contrast, the proteolytic processing of SREBP1, the SREBP family
257 member primarily implicated in unsaturated fatty acid metabolism[49], was not affected by DHA under our
258 conditions. The relationship between these observations and previous reports of PUFA-regulation of
259 SREBPs are expanded upon in the Discussion.

260 Our findings suggested that processing of SREBP2 is involved in homeostatic membrane lipid remodeling
261 in response to perturbation by PUFA incorporation. To test this inference, we measured the response to
262 PUFA supplementation in cells where SREBP processing was inhibited either genetically or
263 pharmacologically. SRD-12B cells are clonal variants of CHO cells wherein a genetic defect in the Site 1
264 Protease (S1P; cleaves SREBPs to produce the transcriptionally active forms) prevents SREBP
265 processing/activation [50]. In these cells, no notable upregulation of cholesterol (Fig 4F) or saturated lipids
266 (Fig S7) was observed upon DHA supplementation. Similarly, chemical inhibition of SREBP activation
267 by the pentacyclic triterpene betulin[51] abrogated DHA-induced upregulation of cholesterol (Fig 4B,
268 triangles). It is important to point out that S1P also processes other important signaling proteins like ATF6,
269 responses that would be abrogated in SRD-12B cells (though likely not by betulin treatment). However,
270 we did not observe induction of ATF6 proteolytic processing by DHA (Fig S8A). We also observed no
271 significant upregulation of the ATF6 target gene Grp78. Finally, we did not observe induction of HSP90B
272 (ER stress response gene) or processing of XBP1, suggesting that ER stress is not significantly induced
273 by DHA feeding (Fig S8B). While these results support a role for SREBP2 processing in PUFA-induced
274 lipidome remodeling, they explicitly do not rule out other contributors to the homeostatic response. Nor

275 do they implicate SREBP2 as the sensor for membrane fluidity. Rather, they establish SREBP2 as an
276 important node of the homeostatic response, and one that can be manipulated to evaluate the cellular
277 consequences of disruptions in membrane homeostasis.

278 One possible explanation for the unexpectedly fast cholesterol response to early stages of DHA
279 accumulation (e.g. 1 h after supplementation) is that DHA-containing lipids are highly fluidizing, even at
280 relatively minor relative abundances [23]. Further, these are likely produced first in the ER and may
281 accumulate at the site of synthesis to much higher levels than in total cell membranes. This local
282 perturbation may induce a rapid and potent response by the cholesterol biosynthetic machinery, which has
283 non-transcriptional as well as transcriptional regulation [52]. It is possible that the early phase of this
284 response is mediated by non-transcriptional regulation of already-available enzymes, whereas the latter
285 phases (including the acyl chain remodeling and increase in saturated lipids) are dependent on
286 transcriptional upregulation of the various machineries.

287

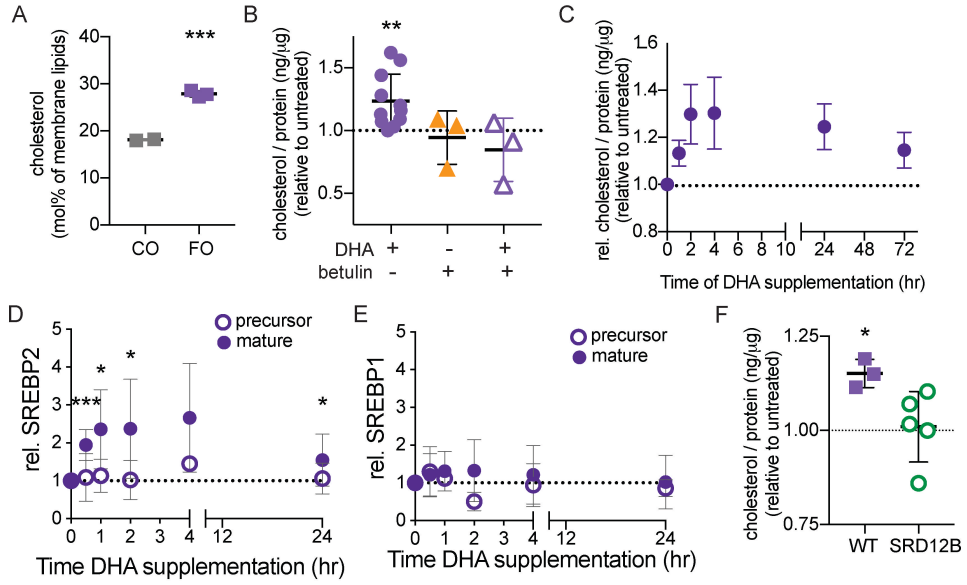

288

289 **Fig 4 – Cholesterol upregulation by DHA supplementation.** (A) Cholesterol levels are higher in membranes isolated from
290 murine heart tissue after feeding with FO compared to CO. (B) Membrane cholesterol is significantly increased by DHA
291 supplementation of cultured RBLs. Effect is abrogated by simultaneous treatment with 200 nM betulin. (C) Time course suggests
292 cholesterol increase is a rapid response to DHA-mediated membrane perturbation. (D) The 'mature', transcription-competent
293 form of SREBP2 is rapidly produced in response to DHA supplementation (full representative Western blots show in Fig S6). (E)
294 SREBP1 proteolytic processing is not significantly affected by DHA supplementation. (F) Cholesterol is significantly increased
295 in WT CHO cells treated with DHA; this effect is abrogated in cells with a defect in SREBP activation (SRD12B; S1P-negative).

296 All data shown are average +/- SD for n ≥ 3 biological replicates; ***p<0.001 in (A) is one-sample t-test between groups; *p<0.05,
297 **p<0.01, ***p<0.001 in B, D, and F are one-sample t-tests compared to untreated.

298

299 *Physical homeostasis following lipidomic perturbation*

300 The above data reveal rapid and comprehensive lipidomic remodeling resulting from the incorporation of
301 DHA into membrane lipids, wherein lipids that decrease membrane fluidity / increase membrane packing
302 (saturated lipids and cholesterol) are rapidly upregulated in response to introduction of PUFA-containing
303 lipids that increase membrane fluidity. These changes are consistent with lipidome remodeling for
304 homeostatic maintenance of membrane physical properties. To directly evaluate this inference, we
305 measured membrane packing in live cells using a fluorescence assay that relies on a solvatochromic dye
306 (C-Laurdan) whose spectral characteristics are dependent on membrane properties [53]. Specifically, the
307 emission spectrum of C-Laurdan is red-shifted in loosely-packed membranes (due to the enhanced polarity
308 of the fluorophore nano-environment), and the relative extent of this spectral shift can be quantified by
309 ratiometric spectroscopy or imaging [54]. The resulting dimensionless parameter called Generalized
310 Polarization (GP) is a widely used proxy for membrane packing and fluidity [55-59], with higher values
311 reporting more tightly packed membranes.

312 The GP of homogenized cell membranes was not significantly affected by 24 h supplementation with
313 DHA, nor by betulin alone. In contrast, the combination of DHA+betulin significantly reduced lipid
314 packing (Fig. 5A). Similarly, while wild-type CHO cells did not show a significant effect of DHA on
315 membrane fluidity after 24 h treatment, DHA supplementation of SRD-12B cells significantly reduced
316 GP (Fig 5B). These measurements of lipid packing in homogenized whole cell membranes suggested that
317 inhibition of lipidomic remodeling prevents the homeostatic maintenance of membrane physical
318 properties.

319 To gain deeper temporal and spatial insight into DHA-mediated lipidomic remodeling, we used confocal
320 spectral imaging [60] to image C-Laurdan GP in cells. Figure 5C shows two-dimensional GP maps of DHA
321 and/or betulin-treated RBL cells with relatively fluid (low GP; blue/green pixels) internal membranes and
322 relatively packed plasma membranes (high GP; yellow/red pixels) characteristic of mammalian cells [54,56].
323 The clearly distinct GP regions enabled us to separately quantify the effects of DHA on plasma versus
324 internal membranes. Figures 5D-E show the GP histograms from the regions within the dotted lines in Fig
325 5C, representing internal membranes. The packing of these internal membranes was significantly
326 decreased shortly after introduction of exogenous DHA (Figs 5F purple circles; pooled data for 2 and 4 h

327 time points are different from 0 with $p < 0.01$), suggesting reduced packing consistent with the expected
328 fluidizing effect of PUFA-containing lipids [23,61]. This response eventually reversed, with GP fully
329 normalizing to baseline by 24 h (Fig. 5F). Thus, DHA incorporation combined with the associated
330 remodeling produced no net change in overall membrane properties. GP at the plasma membrane (PM)
331 was not significantly affected by DHA treatment (Fig 5G). However, we point out that all lipidomic
332 remodeling effects described above for whole cell membranes were also observable in isolated PMs [23].
333 Namely, supplemented PUFAs accumulate in PM lipids, which are then apparently compensated for by
334 increases in saturated lipids and cholesterol (Fig S9). One possible explanation for why PMs showed
335 smaller biophysical changes than internal membranes is that exogenous PUFAs are preferentially
336 incorporated into lipids at the ER, which is site of most lipid synthesis. If lipidome remodeling occurs
337 faster than the trafficking of newly synthesized lipids to the PM, then biophysical disruptions to the PM
338 may be minimal.

339 The re-normalization of membrane packing was markedly abrograted when lipidomic remodeling was
340 inhibited by targeting SREBP processing. Namely, betulin treatment suppressed the recovery of internal
341 membrane packing following DHA treatment, leading to significantly reduced GP in DHA+betulin-
342 treated RBL cells after 24 h (Fig 5C-F, orange symbols and line). The persistently increased fluidity
343 resulting from combined betulin+DHA treatment was observed not only in internal membranes, but also
344 in the PMs (Fig 5G).

345 To more precisely validate the biophysical perturbation of the PM, we employed a recently characterized
346 method that relies on a fluorescent reporter of membrane packing (Di-4-ANEPPDHQ, Di4) that integrates
347 solely into the outer leaflet of the PM (Fig 5H) [62]. Similar to C-Laurdan, the photophysical characteristics
348 of Di4 are dependent on lipid packing, with fluorescence emission lifetime providing a particularly
349 sensitive readout, with higher lifetimes indicative of more tightly packed membranes [62,63]. While neither
350 DHA nor betulin alone significantly affected Di4 lifetime (τ_{Di4}), plasma membrane packing was
351 significantly reduced in DHA+betulin-treated RBL cells (Fig 5H-I).

352 Although biophysical membrane perturbations likely have several distinct physiological effects, we
353 considered the central role of the plasma membrane as a selective barrier. Significant computational and
354 model membrane literature[64,65] suggests that membrane permeability is dependent on lipid composition,
355 with more loosely packed, fluid membranes being more permeable to various polar and amphiphilic
356 compounds. Simulations have specifically analyzed polyunsaturated phospholipids, showing DHA-
357 containing membranes are 2-3-fold more permeable than monounsaturated counterparts[64]. Thus, we

358 hypothesized that the permeability of cell membranes would be increased by incorporation of
359 polyunsaturated lipids. To test this possibility, we developed a method to quantitatively evaluate
360 membrane permeability to amphiphilic substrates in living cells. Specifically, we adapted a classical cell
361 viability assay that relies on the passive diffusion of the amphiphilic compound fluorescein diacetate
362 (FDA) through the PM into the cytoplasm, where cellular hydrolases convert it into fluorescent fluorescein
363 whose charge inhibits its diffusion out of the cell[66]. Because the catalytic conversion of FDA is highly
364 efficient[66], the rate of fluorescence increase is a direct readout of FDA flux through the PM. We observed
365 a linear increase in fluorescence over at least the first 10 mins of measurement, consistent with a constant
366 flux (Q), as shown in Fig 5J. The permeability can then be calculated from the flux using Fick's Law (see
367 Methods). The resulting permeability coefficient for FDA was ~2.2×10^{-6} cm/sec, in good agreement with
368 previously reported values in plant cells[67]. Finally, we tested the effects of DHA and/or betulin on PM
369 permeability. Consistent with our hypothesis, cells with uncompensated membrane perturbations (i.e.
370 DHA+betulin) were indeed more susceptible to passive permeation by FDA (Fig 5K).

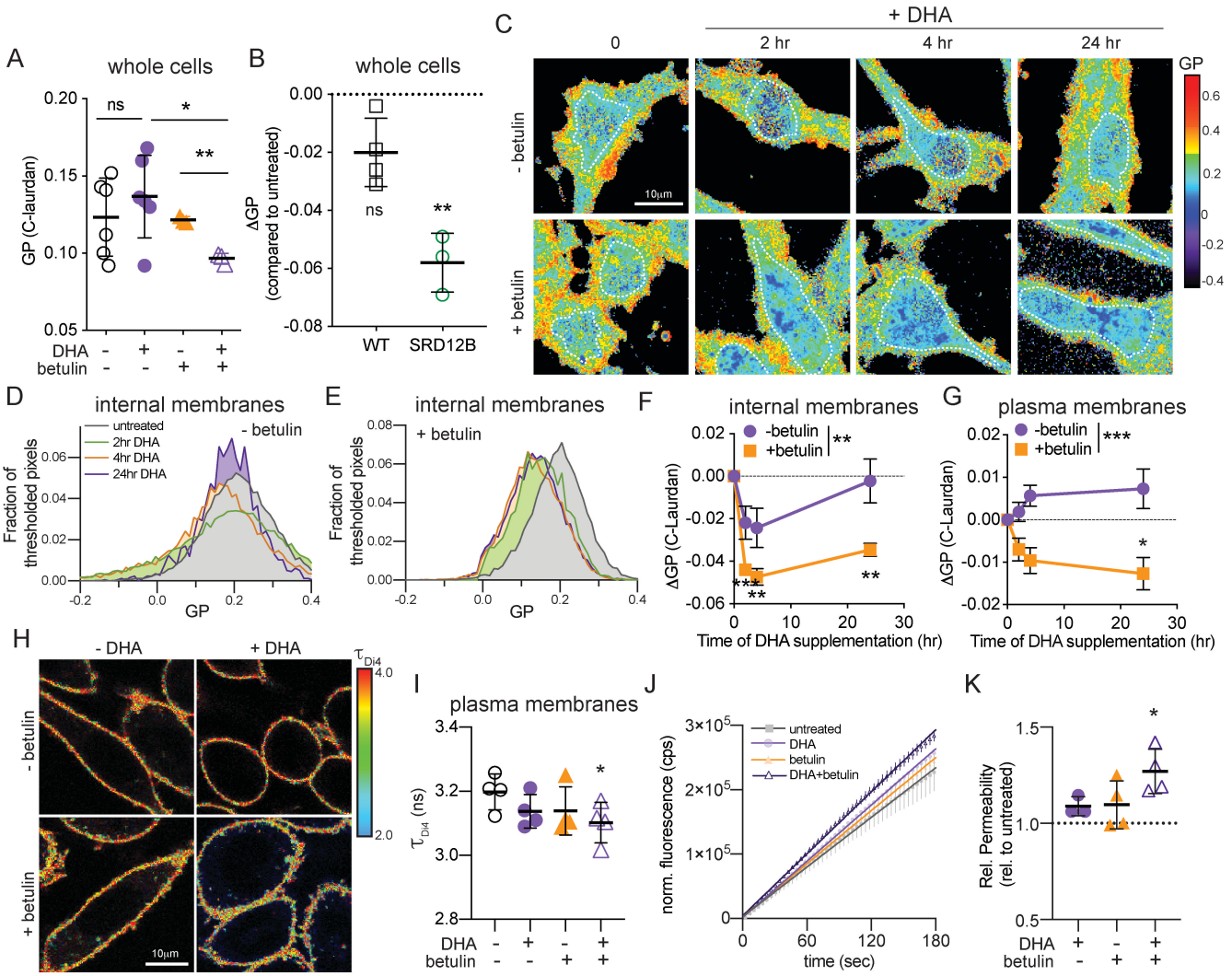

Fig 5 – Physical membrane homeostasis is disrupted by inhibition of lipidomic response. (A) Spectroscopy of C-Laurdan-labeled homogenized whole cell membranes shows that neither DHA nor betulin alone affected membrane packing (GP) after 24 h, whereas DHA+betulin significantly reduced membrane packing. *p<0.05, **p<0.01 is calculated by students t-test between groups. (B) Spectroscopy of C-Laurdan-labeled membranes from WT CHO cells revealed no effect of DHA supplementation after 24 h, whereas SRD-12B cells (defective in SREBP processing) had significantly reduced membrane packing. **p<0.01 one-sample t-tests compared to untreated. (C) Exemplary GP maps of RBL cells treated with DHA and/or betulin demonstrate temporal changes in lipid packing (GP). Images show the characteristically tighter lipid packing (i.e. greater GP) of the PM compared to internal membranes. The white dotted lines denote the areas from which the GP of the internal membranes was calculated. GP histograms of internal membranes from images in A are shown in D-E. Leftward shift in histograms denotes less tightly packed, more fluid membranes. (D) In control cells, internal membranes initially fluidized by excess DHA-containing lipids (green) recovered to baseline by 24 h (purple). (E) In contrast, internal membrane packing did not recover in betulin-treated cells. (F-G) Experiments in C-E were repeated at least 4 times and the mean ± SD (normalized to GP without DHA) is shown. Internal membranes are initially fluidized by excess DHA-containing lipids (purple), then recover to baseline by 24 h. In contrast, internal membrane packing does not recover in betulin-treated cells (orange). The effect of treatment was significant (p<0.01)

387 by 2-way ANOVA, and each time point for betulin-treated cells was significantly different from zero ($p<0.01$). These conclusions
388 were independent of the areas used to calculate internal membrane GP (see Methods). (G) DHA supplementation had no
389 significant effect on packing at the plasma membrane (PM); however, when betulin is added to inhibit lipidomic remodeling, the
390 PM also becomes significantly more fluid upon DHA supplementation. The effect of betulin treatment in PMs was significant
391 ($p<0.001$) by 2-way ANOVA. ΔGP represents GP of treated cells normalized to untreated cells within each experiment. *$p<0.05$,
392 **$p<0.01$, ***$p<0.001$ in D-E of individual time points is calculated by one-sample t-test compared to ΔGP=0. (H) Fluorescence
393 lifetime imaging of Di4 to probe membrane packing in the PM. Warmer colors are representative of higher lifetimes, indicative
394 of more tightly packed membranes. RBL cells were treated for 24 h prior to imaging. (I) Only the combined DHA+betulin treatment
395 significantly reduced Di4 lifetime, consistent with reduction of PM packing. *$p<0.05$ compared to untreated using paired t-tests.
396 (J) Exemplary plots of accumulation of fluorescein fluorescence during incubation with FDA. Shown are average +/- SD of
397 biological repeats and linear regressions. (K) PM permeability to FDA increases by treatment with DHA+betulin. Average +/-
398 SD for $n \geq 3$ biological replicates. **$p<0.01$ is calculated by one-sample t-tests compared to untreated.

399

400 *Disruption of membrane homeostasis induces non-apoptotic cell death*

401 In unicellular organisms, the homeoviscous lipidomic response is believed to be necessary for maintaining
402 membrane physical properties in a range compatible with life [13,15]. Having observed similar lipidomic and
403 biophysical responses in mammalian membranes, we hypothesized that this adaptation was necessary for
404 cellular fitness following membrane perturbations. To test this hypothesis, we evaluated the cytotoxic
405 effects of DHA under pharmacological or genetic inhibition of homeostatic responses produced by
406 SREBP2. At low doses (up to 20 μM DHA and 500 nM betulin), neither DHA nor betulin alone showed
407 significant cytotoxicity; however, DHA supplementation in the presence of betulin led to ~50% decrease
408 in cell number after 3 days of culture (Fig 6A; full dose-response in Supp Fig S10A). We then tested
409 whether the cytostatic effect shown in Fig 6A was due to reduced proliferation or increased cell death. We
410 found that the populations of cells at various parts of cell cycle progression were unaffected by any of the
411 treatments (Fig S11), suggesting that reduced proliferation rates were not the cause of lower cell numbers.
412 We also did not observe an accumulation of sub-G0 cells, which are reflective of DNA fragmentation,
413 often associated with apoptosis. However, the combination of DHA and betulin (but neither treatment
414 alone) significantly increased the proportion of trypan blue positive (TB+) (i.e. dead) cells (Fig 6B). These
415 observations were confirmed in SRD-12B cells, whose genetic lesion renders them incapable of activating
416 SREBP [50] and mounting an adaptive lipidomic and biophysical response to DHA supplementation (Figs
417 4F and 5G). Consistent with the abrogated homeostatic response, DHA had a significant cytotoxic effect
418 on SRD-12B cells (Fig 6C-D, green). Thus, the reduced cellular viability resulting from uncompensated
419 membrane perturbations is due to cytotoxicity.

420 Consistent with increased cell death, we observed a significantly increased fraction of propidium iodide
421 positive (PI+) cells after 24 hrs of combined DHA+betulin treatment (Fig 6E and I). Despite the lack of
422 sub-G0 cells, we speculated that apoptosis was possibly involved in inducing cell death, perhaps resulting
423 from imbalanced signaling at the PM or membrane stress induced by lipidomic perturbations. One
424 hallmark of apoptosis is the externalization of PS (marked by Annexin V) without loss of membrane
425 integrity (marked by PI), allowing apoptotic cells to be identified as AnxV+ / PI- by flow cytometry. After
426 24 h of treatment with DHA and/or betulin, we observed no significant increases in AnxV+ / PI- cells (Fig
427 6F-I), suggesting that the increased cell death was not apoptotic. Consistently, using a fluorescent marker
428 of active caspases (CellEvent Caspase-3/7), we observed no induction of apoptosis in cells treated with
429 DHA+betulin (Fig S12A). Finally, the involvement of apoptosis in a cytotoxic process can be inferred by
430 using potent caspase inhibitors (e.g. Z-VAD-FMK), which should attenuate apoptosis-induced
431 cytotoxicity. Treatment with this inhibitor did not inhibit cell death (Fig S12B), supporting a non-apoptotic
432 cytotoxicity mechanism.

433 Together, these results reveal that inhibition of lipidome remodeling in mammalian cells markedly
434 increased non-apoptotic cell death upon membrane perturbation with dietary fatty acids. Because cell
435 physiology is essentially dependent on maintaining cytoplasmic concentrations of a plethora of small
436 molecules (water, alcohols, polyamines) and amphiphiles (steroids, fatty acids) that can passively diffuse
437 through the membrane, it is possible that the significant increases in membrane permeability (Fig 5H-I)
438 may be responsible for the observed toxicity.

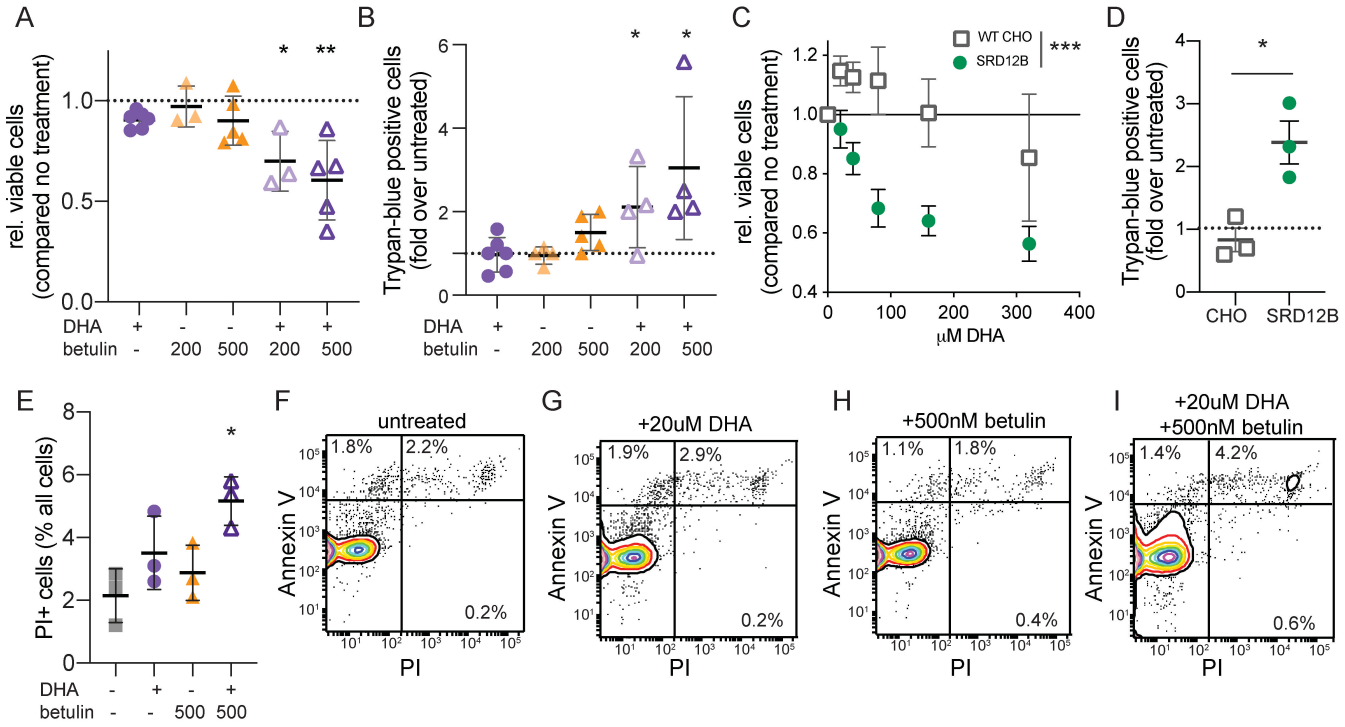

Fig 6 – Inhibition of homeostatic lipidome remodeling induces non-apoptotic cytotoxicity. (A) Neither DHA nor betulin alone had a significant cytotoxic effect in RBLs, whereas their combination significantly reduced viability. (B) 24hr of DHA+betulin treatment significantly increased the number of trypan-positive cells. (C) In SRD-12B cells, which fail to upregulate cholesterol and saturated lipids upon DHA treatment (see Fig 4D and Supp Fig S6), DHA significantly inhibited cell growth, in contrast to control WT CHO cells. (D) In SRD-12B cells, DHA significantly increased the proportion of TB+ cells, in contrast to WT CHO cells. (E) DHA+betulin treatment for 24 hr significantly increased the proportion of PI+ cells. (F-I) Flow cytometry showed no increase in AnxV+/PI- cells (reflective of apoptosis), while the AnxV+/PI+ cells (non-apoptotic cell death) were increased. Flow cytometry positive controls shown in Fig S13. All data shown as mean +/- SD for ≥ 3 independent experiments. A, B, and D are one-sample t-tests compared to untreated; E is student's t-test compared to untreated; C is two-way ANOVA for effect of treatment. *p<0.05, **p<0.01, ***p<0.001.

DISCUSSION

The incorporation of dietary fatty acids into mammalian membrane lipids has been widely observed both *in vitro* [23,68,69] and *in vivo* [19,20,37,38,70]. The fact that exogenous fatty acids are so readily used for lipid synthesis is unsurprising in light of the fact that the enzyme required for *de novo* fatty acid production (fatty acid synthase) is minimally expressed in most adult human tissues [71]. Indeed, *de novo* lipogenesis is considered "negligible" [72,73] in adult humans, suggesting that exogenous sources of fatty acids are the major raw material for maintenance and replenishment of membrane lipids. This reliance on exogenous

458 inputs for production of components central to cellular architecture and function would seem to present a
459 major complication for homeostasis.

460 In ectothermic organisms, homeostatic membrane control has been widely reported in the form of
461 homeoviscous adaptation (HVA) [13-15]. According to this hypothesis, the relative abundance of saturated
462 to unsaturated membrane lipids is responsive to temperature changes in order to maintain membrane
463 fluidity at the level required for the many processes hosted and regulated by cell membranes. Although
464 such adaptation has been proposed in prokaryotes [14], single-celled eukaryotes [74], and even cold-blooded
465 animals [75,76], studies on endothermic organisms have been limited [28,29], and there has yet been no direct
466 observations of HVA in mammals or isolated mammalian cells. Our data directly confirm all major tenets
467 of cell-autonomous homeoviscous adaptation: (1) lipidomic remodeling resulting from a perturbation of
468 membrane physical properties (Fig 2-4); (2) recovery of baseline physical properties at a new lipid
469 composition (Fig 5); and (3) necessity of this response for cellular fitness (Fig 6). These observations
470 suggest that mammalian cells possess the capacity for homeostatic membrane adaptation analogous to
471 HVA, and that this response can compensate for perturbations from dietary lipid inputs.

472 In cold-blooded animals, the homeostatic membrane response also involves modulation of cholesterol
473 levels [48,76], and we observe a similar response in mammalian cells, mediated at least partially through
474 activation of SREBP2 (Fig 4). Disruption of SREBP activation resulted in inhibition of the compensatory
475 response, both with respect to lipid composition (Figs 3 and 4, and Supp Fig S7) and biophysical properties
476 (Fig 5). The implication of SREBP2 as a node of the sense-and-respond module for membrane adaptation
477 is consistent with the central role of SREBPs in membrane homeostasis [49]. SREBP transcription factors
478 have been dubbed the "master regulators of lipid homeostasis", because they direct not only cholesterol
479 synthesis and uptake, but also proteins associated with membrane lipid metabolism, including those
480 involved in FA synthesis, elongation, and desaturation [77]. The effects of PUFA supplementation on
481 SREBP signaling have been extensively studied, and DHA is known to suppress the activation of SREBP1
482 and its target genes, both in cultured cells and *in vivo* [78-80]. In contrast, SREBP2 is not suppressed by
483 PUFAs [78,79], revealing that these two complementary regulators of membrane homeostasis have different
484 functions, despite both being sensitive to membrane cholesterol. In our observations, SREBP2 is
485 proteolytically activated as part of the homeostatic response. Previous reports [79] have not noted a
486 significant effect of PUFAs on SREBP2, possibly because those experiments involved acute PUFA
487 feeding of serum-starved cells, where high levels of activated SREBPs may have suppressed the DHA-
488 mediated stimulation we observe. We have confirmed the possibility for such an effect in our cells (Fig
489 S14). It remains to be determined whether SREBP2 is simply an effector of membrane remodeling

490 downstream of yet-unidentified sensing machinery, or whether this protein (and/or its regulatory
491 machinery) may itself be capable of sensing perturbations in membrane physical properties. Direct
492 demonstration of protein responsiveness to membrane packing has recently been described for two yeast
493 ER proteins [5,18], providing a conceptual and methodological toolbox for identifying other membrane
494 sensors. Remarkably, despite the ubiquity and importance of membrane homeostasis, the machinery used
495 for sensing membrane properties remains largely uncharacterized. It is an intriguing observation that Ire1,
496 a core component of the unfolded protein response (UPR), exhibits a dual sensitivity to unfolded proteins
497 and aberrant lipid compositions, demonstrating a tight connection between protein-folding and membrane
498 properties [18]. This connection suggests that the machinery for ameliorating protein-folding stresses may
499 also be involved in transducing and mitigating membrane stress [81].

500 With extensive literature on the effects of dietary lipids on membrane compositions [36,37,82-84], it is somewhat
501 surprising that the remodeling we observe has not been previously reported. We note that in many of the
502 published datasets, increases in saturated fatty acids have indeed been observed, though rarely remarked
503 upon. We speculate that the compensatory effects may have been previously overlooked for several
504 reasons: (a) remodeling effects are obviously less pronounced than the "main" effects (incorporation and
505 substitution) and may have been considered incidental/irrelevant; (b) lipid remodeling is temporally
506 regulated and the time point of sample collection may affect its magnitude [84]; (c) most previous reports
507 have analyzed isolated FAs rather than intact lipids, which may obscure how these are combined into
508 phospholipids (e.g. it is possible to have more fully saturated lipids without a major increase in saturated
509 FAs); (d) remodeling of the non-supplemented FAs can be obscured by the high abundance of the
510 supplemented FAs. For example, if a large fraction of the phospholipidome is converted into DHA-
511 containing lipids by DHA feeding, then the mol fraction of other lipids obviously decreases, even if the
512 relative proportion of saturated acyl chains compared to unsaturated is increased; (e) cholesterol is rarely
513 considered alongside FAs and is a major component of the remodeling we report.

514 In summary, our observations support the hypothesis that mammalian cells in culture and *in vivo* sense
515 membrane physical properties and respond to perturbations by comprehensive remodeling of their
516 lipidomes. In our measurements, the perturbations were induced by supplementation with polyunsaturated
517 fatty acids (PUFAs); however, it is likely that other fats (e.g. cholesterol) or amphiphiles (bile acids,
518 anesthetics) may induce similar responses. We show that the compensatory response is necessary for cell
519 fitness, confirming membrane adaptation as a central requirement for cellular homeostasis.
520

521 **MATERIALS AND METHODS**

522 ***Materials:*** DHA, AA, OA, PA,_betulin, GSK2194069, PF-429242, fluorescein diacetate, and 1,10
523 phenanthroline were obtained from Sigma Aldrich. C-Laurdan was purchased from TPProbes (South
524 Korea). Amplex Red kit to quantify cholesterol was purchased from Invitrogen. Antibodies used: actin
525 (monoclonal clone AC-15, Abcam), SREBP2 (polyclonal, Abcam), SREBP1 (monoclonal, Abcam). Z-
526 DEVD-FMK and myriocin was purchased from Cayman Chemicals). Di-4-ANEPPDHQ (Di4),
527 CellEvent™ Caspase-3/7 Green Detection Reagent, Annexin V-Pacific Blue, and Hoechst 33342 was
528 purchased from ThermoFisher. Fluorescein sodium salt was purchased from Santa Cruz Biotechnology.

529

530 ***Cell culture:*** Rat basophilic leukemia (RBL) cells were maintained in medium containing 60% modified
531 Eagle's medium (MEM), 30% RPMI, 10% fetal calf serum, 100 units/mL penicillin, and 100 μg/mL
532 streptomycin. Chinese hamster ovary (CHO) cells were maintained in DMEM:F12 (1:1) containing 5%
533 fetal calf serum, 100 units/mL penicillin, and 100 μg/mL streptomycin. SRD12B cells were maintained
534 in DMEM:F12 (1:1) containing 5% fetal calf serum, 50μM sodium mevalonate, 20μM oleic acid, 5μg/mL
535 cholesterol, 100 units/mL penicillin, and 100 μg/mL streptomycin, as previously described[85]. All cells
536 were grown at 37ºC in humidified 5% CO2.

537

538 ***Fatty acid treatments:*** Fatty acid stock solutions were received as air-purged ampules (Sigma Aldrich)
539 and loaded into BSA immediately upon opening. BSA loading was accompanied by stirring the fatty acid
540 with BSA dissolved in water (2:1 mol/mol FA:BSA), sterile filtering, purging with nitrogen prior to
541 aliquoting, and storing at -80°C. BSA loading, purging, and cold storage were all done to minimize FA
542 oxidation. For all experiments with FA supplementation, cells were incubated with 20 μM FA for 3 days
543 (cells were re-supplemented 24 h prior to analysis). Serum-containing, rather than serum-free, media was
544 used to approximate physiological supplementation, rather than exclusive introduction of specific FAs.
545 These conditions were chosen to approximate *in vivo* settings produced by DHA-enriched diets in
546 mammals: plasma free FA concentrations range from 300 to 750 μM [70,86] and up to 10 mol % of plasma
547 fatty acids are ω-3 DHA in rats fed a high-fish-oil diet [70]. Further, diets rich in ω-3 PUFAs led to
548 significant incorporation of these fats into cell membrane lipids [19,38,70], similar to the levels we observed
549 under our culture feeding conditions (Fig. 1). For these reasons, we believe our culture conditions
550 reasonably approximate physiological dietary membrane perturbations.

551

552 ***Animals and diets:*** All experimental procedures using laboratory animals were approved by the Public
553 Health Service and the Institutional Animal Care and Use Committee at Texas A&M University.
554 Pathogen-free female C57BL/6 mice (n=8) weighing 16–18 g, were randomly divided into two groups of
555 4. For 2 weeks, mice had free access to one of the two semi-purified diets, which were adequate in all
556 nutrients [36]. Diets varied only in the oil composition, i.e., either corn oil (CO) or a PUFA-enriched fish-
557 corn oil (FO) mixture (4:1, w/w) at 5 g/100 g diet. The basic diet composition, expressed as g/100 g was:
558 casein, 20; sucrose, 42; cornstarch, 22; cellulose, 6; AIN-76 mineral mix, 3.5; AIN-76 vitamin mix, 1,
559 DL-methionine, 0.3; choline chloride, 0.2; Tenox 20A, 0.1; and oil, 5. The fatty acid composition of the
560 diets was determined by gas chromatography (Supplemental Table 1). Mice were sacrificed by CO2
561 asphyxiation after two weeks of feeding the CO/FO diet, and the livers and hearts were frozen in liquid
562 nitrogen. 20-50 mg of tissue was mechanically homogenized in Dulbecco's PBS (without Ca^{2+} and Mg^{2+}).
563 Samples were further diluted to 5 mg/mL in Dulbecco's PBS (without Ca^{2+} and Mg^{2+}), and lipidomics
564 analysis was performed as below.

565

566 ***Drug treatments and cell number quantification:*** RBL cells were treated with or without 20 μM DHA
567 in the presence or absence of betulin (inhibitor of SREBP processing) or GSK2194069 (FAS inhibitor).
568 Cells were treated for 72 h, and then the cell number determined via fluorescein diacetate (FDA)
569 fluorescence. FDA is a cell viability probe which freely diffuses through cell membranes but is trapped in
570 cells following de-acytelation by cytoplasmic esterases in viable cells. The number of viable cells is then
571 directly related to fluorescein fluorescence intensity. For the assay, cells were treated in 96-well plates,
572 gently washed with PBS, and then incubated with fluorescein diacetate (5 μg/mL in PBS) for 2 minutes
573 at 37°C. The plates were then washed again to remove excess FDA and fluorescence was measured at 488
574 nm excitation and 520 nm emission. For caspase inhibitor studies, 5 and 30 μM Z-DEVD-FMK were
575 added at the same time as DHA and betulin and treated for 72 h prior to FDA analysis.

576 To count the number of dead cells, cells were treated for 24 h, and the supernatant harvested. The cells
577 were then trypsinized and combined with the supernatant. 0.4% Trypan Blue was added to an equal
578 volume of cells. The cells were then counted using a Countess II cell counter (Thermo Fisher), and the
579 number of Trypan-positive cells recorded. For each experiment the number of cells per well were
580 normalized to untreated, unsupplemented cells.

581

582 ***Active caspase quantification:*** RBL cells were treated with or without 20 μM DHA in the presence or
583 absence of 500nM betulin for 24 h. After 24hr, the supernatant was removed, and CellEvent™ Caspase-
584 3/7 Green Detection Reagent (7.5 μM, diluted in PBS + 0.5% FBS) was added to each well. The cells
585 were incubated at 37°C for 30 min. At this time Hoechst 33342 (2.5μg/mL final) was added to the solution
586 and incubated for an addition 5 min at 37°C. Two images using DAPI and GFP filters were randomly
587 taken for each condition in three different random locations in the well. For a positive control, cells were
588 treated with 2 mM N-ethylmaleimde in 50 mM HEPES, 2 mM CaCl2, pH 7.4 for 45 min prior to addition
589 of the caspase detection reagent. Using ImageJ, to determine positive staining for caspase activity, a
590 threshold was set using the positive controls, and this threshold was maintained across the experiment.
591 The number of caspase-positive cells was normalized to the number of cells imaged in the same field of
592 view by counting the Hoechst-positive nuclei.

593

594 ***Lipidomics:*** Detailed lipidomic analysis was performed by Lipotype, GmbH, as previously described[87].
595 Briefly, for preparation of crude cell membranes, cells were washed with phosphate buffered saline (PBS),
596 scraped in 10 mM Tris pH 7.4, and then homogenized with a 27-gauge needle. Nuclei were then pelleted
597 by centrifugation at 300 xg for 5 min. The supernatant was pelleted by centrifugation at 100,000 xg for 1
598 h at 4°C. The membrane pellet was then washed and resuspended in 150 mM ammonium bicarbonate.

599 All lipidomics were performed at Lipotype GmbH (Dresden, Germany) as described previously [21-23,26,34,88]
600 and detailed below.

601 Nomenclature: The following lipid names and abbreviations are used: ceramide (Cer), Chol, SM,
602 diacylglycerol (DAG), lactosyl ceramide (DiHexCer), glucosyl/galactosyl ceramide (HexCer), sterol ester
603 (SE), and triacylglycerol (TAG), as well as phosphatidic acid (PA), phosphatidylcholine (PC),
604 phosphatidylethanolamine (PE), phosphatidylglycerol (PG), and phosphatidylinositol (PI),
605 phosphatidylserine (PS), and their respective lysospecies (lysoPA, lysoPC, lysoPE, lysoPI, and lysoPS)
606 and ether derivatives (PC O-, PE O-, LPC O-, and LPE O-). Lipid species were annotated according to
607 their molecular composition as follows: [lipid class]-[sum of carbon atoms in the FAs]:[sum of double
608 bonds in the FAs];[sum of hydroxyl groups in the long chain base and the FA moiety] (e.g., SM-32:2;1).
609 Where available, the individual FA composition according to the same rule is given in brackets (e.g.,
610 18:1;0-24:2;0).

611 <u>Lipid standards:</u> Synthetic lipid standards were purchased from Sigma-Aldrich (Chol D6), Larodan
612 (Solna, Sweden) Fine Chemicals (DAG and TAG), and Avanti Polar Lipids (all others).

613 Lipid extraction for mass spectrometry lipidomics: Lipids were extracted using a two-step
614 chloroform/methanol procedure [26]. Samples were spiked with internal lipid standard mixture containing:
615 cardiolipin 16:1/15:0/15:0/15:0 (CL), ceramide 18:1;2/17:0 (Cer), diacylglycerol 17:0/17:0 (DAG),
616 hexosylceramide 18:1;2/12:0 (HexCer), lyso-phosphatidate 17:0 (LPA), lyso-phosphatidylcholine 12:0
617 (LPC), lyso-phosphatidylethanolamine 17:1 (LPE), lyso-phosphatidylglycerol 17:1 (LPG), lyso-
618 phosphatidylinositol 17:1 (LPI), lyso-phosphatidylserine 17:1 (LPS), phosphatidate 17:0/17:0 (PA),
619 phosphatidylcholine 17:0/17:0 (PC), phosphatidylethanolamine 17:0/17:0 (PE), phosphatidylglycerol
620 17:0/17:0 (PG), phosphatidylinositol 16:0/16:0 (PI), phosphatidylserine 17:0/17:0 (PS), cholesterol ester
621 20:0 (CE), sphingomyelin 18:1;2/12:0;0 (SM), triacylglycerol 17:0/17:0/17:0 (TAG) and cholesterol D6
622 (Chol). After extraction, the organic phase was transferred to an infusion plate and dried in a speed vacuum
623 concentrator. 1st step dry extract was re-suspended in 7.5 mM ammonium acetate in
624 chloroform/methanol/propanol (1:2:4, V:V:V) and 2nd step dry extract in 33% ethanol solution of
625 methylamine in chloroform/methanol (0.003:5:1; V:V:V). All liquid handling steps were performed using
626 Hamilton Robotics STARlet robotic platform with the Anti Droplet Control feature for organic solvents
627 pipetting.

628 MS data acquisition: Samples were analyzed by direct infusion on a QExactive mass spectrometer
629 (Thermo Scientific) equipped with a TriVersa NanoMate ion source (Advion Biosciences). Samples were
630 analyzed in both positive and negative ion modes with a resolution of $R_{m/z=200}$=280000 for MS and
631 $R_{m/z=200}$=17500 for MS/MS experiments, in a single acquisition. MS/MS was triggered by an inclusion list
632 encompassing corresponding MS mass ranges scanned in 1 Da increments [88]. Both MS and MS/MS data
633 were combined to monitor CE, DAG and TAG ions as ammonium adducts; PC, PC O-, as acetate adducts;
634 and CL, PA, PE, PE O-, PG, PI and PS as deprotonated anions. MS only was used to monitor LPA, LPE,
635 LPE O-, LPI and LPS as deprotonated anions; Cer, HexCer, SM, LPC and LPC O- as acetate adducts and
636 cholesterol as ammonium adduct of an acetylated derivative [89].

637 <u>Lipid identification and quantification:</u> Data were analyzed with in-house developed lipid identification
638 software based on LipidXplorer (20). Data post-processing and normalization were performed using an
639 in-house developed data management system. Only lipid identifications with a signal-to-noise ratio >5,
640 and a signal intensity 5-fold higher than in corresponding blank samples were considered for further data
641 analysis.

642 <u>Lipidomics data processing:</u> The lipidomic analysis yields a list of >600 individual lipid species and their
643 picomolar abundances. These were processed by first transforming into mol% of all lipids detected. Next,

644 the TAG and sterol esters were removed from the analysis, and the remaining data was analyzed as mol%
645 of membrane lipids. From here, the datasets were broken down further into class composition. In some
646 cases, the distribution and structural characteristics (e.g. number of carbons or unsaturations in the acyl
647 chains) of the individual species were analyzed.

648

649 *Lipidomic results presentation:* Both DHA and AA can be converted into other PUFAs. DHA can be
650 retro-converted to EPA (20:5) which can then be converted to 24:6. AA can be converted into 22:4 and
651 24:4. In our supplemented cells, we see small, but non-negligible increases in lipids containing these
652 converted, supplemented fatty acyl chains. With DHA supplementation, the retroconversion represented
653 <4.8 mol% GPLs. With AA supplementation, lipids containing converted FAs range from 13-15%. Thus,
654 ω−3 PUFAs are defind here (Fig 1) as lipids containing either 22:6, 20:5, or 24:6 as an acyl chain. ω−6
655 PUFAs are lipids which contain 20:4, 22:4, or 24:4 as an acyl chain.

656

657 ***C-laurdan spectroscopy:*** Membrane packing (related to order and fluidity) was determined via C-laurdan
658 spectroscopy as described [90,91]. Briefly, cells were washed with PBS and stained with 20 µg/mL C-laurdan
659 for 10 minutes on ice. The emission spectrum from isolated GPMVs was gathered from 400-550 nm with
660 excitation at 385 nm at 23°C. The GP was calculated according to the following equation:
661

662 $$GP = \frac{\sum_{420}^{460} I_x - \sum_{470}^{510} I_x}{\sum_{420}^{460} I_x + \sum_{470}^{510} I_x}$$

663

664 ***C-Laurdan spectral imaging:*** C-Laurdan imaging was performed as previously described [23,34,60,90,91].
665 Briefly, cells were washed with PBS and stained with 10 µg/mL C-Laurdan for 10 min on ice, then imaged
666 via confocal microscopy on a Nikon A1R with spectral imaging at 60x and excitation at 405 nm. The
667 emission was collected in two bands: 433–463 nm and 473–503 nm. MATLAB (MathWorks, Natick,
668 MA) was used to calculate the two-dimensional (2D) GP map, where GP for each pixel was calculated
669 from a ratio of the two fluorescence channels, as previously described [60]. Briefly, each image was binned
670 (2x2), background subtracted, and thresholded to keep only pixels with intensities greater than 3 standard
671 deviations of the background value in both channels. Supplemental Fig 15 shows representative images
672 of each of these image processing steps. The GP image was calculated for each pixel using the above
673 equation. GP maps (pixels represented by GP value rather than intensity) were imported into ImageJ. To

674 ensure that the specifics of our quantification method were not biasing the result, we quantified the GP of
675 internal membranes by three different methods:

676 1. Line scans drawn across individual cells, as shown in the original figure. PM GP values were taken as peak
677 GP values from the periphery of the cell, whereas internal membranes were calculated as the average of all
678 values outside the PM peak.
679 2. The nucleus is visible as a dark spot in C-Laurdan images. We used this as a fiducial marker to draw a
680 region-of-interest representing peri-nuclear membranes and calculated the average GP of those pixels.
681 3. As shown in the images in Figure 5, the internal membranes were masked, and histograms of the pixels
682 inside the mask were plotted.

683 Ultimately, all three methods produced quantitatively similar results, suggesting that this measurement is
684 robust. We chose to present the results of the third method here because it includes the most information,
685 allowing us to evaluate the distributions of pixels GPs.
686

687 ***Di4 fluorescence lifetime imaging:*** Outer leaflet staining of RBL cell PMs was achieved by incubating
688 cells at 4°C for 8 min with Di4 at 1 μg/ml in phosphate-buffered saline. Cells were quickly washed prior
689 to immediate imaging in phenol red-free MEM. Lifetime microscopy was performed on a Nikon A1 laser
690 scanning microscope with an integrated Picoquant time-correlated single photon counting (TC-SPC)
691 system (Berlin, Germany). The instrument response function (IRF) was determined with a saturated
692 erythrosine B and KI solution at pH=10 according to the manufacturer's (Picoquant) protocol. Di4
693 emission was collected at >560 nm, and images were acquired using 20 MHz pulse frequency. The photon
694 count rate was kept under 10% of the pulse rate by adjusting a manual shutter, and enough frames were
695 acquired to obtain at least $8x10^3$ photons cumulative signal intensity. The fluorescence decay curves were
696 fitted to a bi-exponential re-convolution function adjusted to the IRF, and the average lifetime was
697 calculated and represented in the FLIM images as τ_{Di4}. The experiment was repeated 4 times, imaging
698 15-30 cells per condition each time.

699

700 ***Amplex Red assay:*** Amplex Red cholesterol assay was performed (according to manufacturer
701 instructions; Invitrogen) to determine the abundance of cholesterol. Each reading was normalized to
702 protein concentration (determined by bicinchoninic acid (BCA) assay) in the same samples. Technical
703 triplicates were measured for each sample. Shown are values normalized to untreated cells. Reported are
704 the average and standard deviations from at least 3 independent biological replicates.

705

706 ***Western Blot:*** Cells were washed with ice cold PBS, then scraped into Laemmli lysis buffer (50mM Tris-
707 HCl, pH 8.0; 2% SDS; 5mM EDTA, pH8.0) supplemented with protease inhibitor cocktail. Protein
708 concentration was determined using BCA (Pierce), and equal amounts of protein were mixed with
709 reducing Laemmli sample buffer and loaded onto SDS-PAGE gels. Gels were transferred to PVDF
710 membranes, which were blocked in 5% BSA. Membranes were incubated with primary antibodies
711 overnight at 4°C, and detected with either AlexaFluor or HRP-tagged secondary antibodies. Membranes
712 were imaged using a BioRad ChemiDoc imager. The intensities of the bands were quantified normalized
713 to actin, and plotted as mean ± SD of n ≥ 3 experiments.
714
715 ***Real Time Quantitative PCR:*** Total RNA was isolated via Trizol (Sigma) following the manufacturer's
716 protocol. Reverse transcriptase PCR was performed using the High Capacity cDNA Reverse Transcription
717 Kit from Applied Biosystems according to manufacturer's protocol. To quantify mRNA expression,
718 SYBR Fast MasterMix (2x) Universal Dye (#KK4602) from Kapa Biosystems was used in an Eppendorf
719 Realplex2 Mastercycler. Each primer set for each sample was run in triplicate with 1 ng of cDNA per
720 well. The primer sets used are:
721

722

Gene	Forward Primer	Reverse Primer
GAPDH	GTCTACTGGCGTCTTCACCA	GTGGCAGTGATGGCATGGAC
SCD1	GTGATGTTCCAGAGGAGGTACT	CAGGAACTCAGAAGCCCAGAA
SCD2	GGTGATGTTCCAGAGGAGGTATT	AACTGGAAGACCCCGAACTC
Grp78	CTACGAAGGTGAACGACCCC	ATTTCTTCAGGGGTCAGGCG
HSP90B	TAAGCTCTATGTGCGCCGAG	TCATCGGAATCCACAACACCT
sXBP1	CTGAGTCCGCAGCAGGTG	TTCCAGCTTGGCTGATGAGG

723
724 Expression changes were calculated using the delta delta C_T method.
725
726 ***Permeability assay:*** RBL cells were treated with or without 20 μM DHA in the presence or absence of
727 500nM betulin for 24 h. At this time, cells were trypsinized, washed 1x with full serum-containing
728 medium and 2x with phenol red-free MEM, and counted with a Countess II automated cell counter

729 (ThermoFisher). 250,000 cells were diluted in 2 mL with phenol red-free MEM and added to a quartz 2
730 mL cuvette. Just prior to reading on the spectrofluorometer, 2.5 ug/mL fluorescein diacetate (stock 1
731 mg/mL in acetone) was added to the cells and mixed by pipetting. The fluorescence intensity was read at
732 450 nm excitation and 510 nm emission over a period of 5 minutes (1 read / second). In each of the samples
733 measured, the slope of the fluorescence increase over time remained constant over the entire 5 minutes,
734 consistent with a constant flux (Q).

735 The permeability coefficient (P) of a membrane to a particular substrate is then defined by Fick's Law as:
736 $Q = P * A * (C_{out} - C_{in})$

737 where A is the area of the membrane and C_{out} and C_{in} are the concentrations of the solute outside and
738 inside the cells, respectively. In our experiments, $C_{in} = 0$ because FDA is quickly converted into a different
739 molecule upon entering the cell. We estimate the transport surface area by multiplying a typical
740 mammalian cell surface area (~3000 μm^2) by the number of cells in the cuvette (250,000). Using pure
741 fluorescein for calibration, we measured directly the flux of FDA molecules across the membrane, which
742 for a typical sample of untreated RBL cells was 6.6 x 10^{-5} nmol/sec. From these parameters, we calculated
743 a permeability coefficient for FDA to be ~2.2 x 10^{-6} cm/sec, in excellent agreement with values previously
744 reported in plant cells[67]. We found that the flux scales linearly with cell and FDA concentrations,
745 consistent with the simple Fick's Law model of passive diffusion followed by rapid active conversion.

746

747 **Acknowledgements**

748 All fluorescence microscopy was performed at the Center for Advanced Microscopy, Department of
749 Integrative Biology & Pharmacology at McGovern Medical School, UTHealth. We gratefully
750 acknowledge Theodore Steck, Yvonne Lange, and members of the Levental lab for their critical feedback
751 on this manuscript. Funding for this work was provided by the NIH/National Institute of General Medical
752 Sciences (GM114282, GM124072, GM120351), the Volkswagen Foundation (grant 93091), and the
753 Human Frontiers Science Program (RGP0059/2019). All authors have no competing interests.

754

755 **References**

756 1 Krogh, A., Larsson, B., von Heijne, G. & Sonnhammer, E. L. Predicting transmembrane protein topology
757 with a hidden Markov model: application to complete genomes. *Journal of molecular biology* **305**, 567-
758 580, doi:10.1006/jmbi.2000.4315 (2001).

759 2 Janmey, P. A. & Kinnunen, P. K. Biophysical properties of lipids and dynamic membranes. *Trends in cell*
760 *biology* **16**, 538-546, doi:10.1016/j.tcb.2006.08.009 (2006).
761 3 Los, D. A. & Murata, N. Membrane fluidity and its roles in the perception of environmental signals.
762 *Biochim Biophys Acta* **1666**, 142-157, doi:10.1016/j.bbamem.2004.08.002 (2004).
763 4 Andersen, O. S. & Koeppe, R. E., 2nd. Bilayer thickness and membrane protein function: an energetic
764 perspective. *Annu Rev Biophys Biomol Struct* **36**, 107-130,
765 doi:10.1146/annurev.biophys.36.040306.132643 (2007).
766 5 Covino, R. *et al.* A eukaryotic sensor for membrane lipid saturation. *Molecular cell* **63**, 49-59,
767 doi:10.1016/j.molcel.2016.05.015 (2016).
768 6 daCosta, C. J., Dey, L., Therien, J. P. & Baenziger, J. E. A distinct mechanism for activating uncoupled
769 nicotinic acetylcholine receptors. *Nat Chem Biol* **9**, 701-707, doi:10.1038/nchembio.1338 (2013).
770 7 Marsh, D. Protein modulation of lipids, and vice-versa, in membranes. *Biochim Biophys Acta* **1778**, 1545-
771 1575, doi:10.1016/j.bbamem.2008.01.015 (2008).
772 8 Roux, A. *et al.* Membrane curvature controls dynamin polymerization. *Proc Natl Acad Sci U S A* **107**,
773 4141-4146, doi:10.1073/pnas.0913734107 (2010).
774 9 Shi, Z. & Baumgart, T. Membrane tension and peripheral protein density mediate membrane shape
775 transitions. *Nature communications* **6**, 5974, doi:10.1038/ncomms6974 (2015).
776 10 Rosholm, K. R. *et al.* Membrane curvature regulates ligand-specific membrane sorting of GPCRs in
777 living cells. *Nat Chem Biol* **13**, 724-729, doi:10.1038/nchembio.2372 (2017).
778 11 Sezgin, E., Levental, I., Mayor, S. & Eggeling, C. The mystery of membrane organization: composition,
779 regulation and roles of lipid rafts. *Nat Rev Mol Cell Biol* **18**, 361-374, doi:10.1038/nrm.2017.16 (2017).
780 12 Lorent, J. H. *et al.* Structural determinants and functional consequences of protein affinity for membrane
781 rafts. *Nature communications* **8**, 1219, doi:10.1038/s41467-017-01328-3 (2017).
782 13 Hazel, J. R. Thermal adaptation in biological membranes: is homeoviscous adaptation the explanation?
783 *Annu Rev Physiol* **57**, 19-42, doi:10.1146/annurev.ph.57.030195.000315 (1995).
784 14 Sinensky, M. Homeoviscous adaptation--a homeostatic process that regulates the viscosity of membrane
785 lipids in Escherichia coli. *Proc Natl Acad Sci U S A* **71**, 522-525 (1974).
786 15 Ernst, R., Ejsing, C. S. & Antonny, B. Homeoviscous adaptation and the regulation of membrane lipids.
787 *Journal of molecular biology* **428**, 4776-4791, doi:10.1016/j.jmb.2016.08.013 (2016).
788 16 Guschina, I. A. & Harwood, J. L. Mechanisms of temperature adaptation in poikilotherms. *FEBS Lett*
789 **580**, 5477-5483, doi:10.1016/j.febslet.2006.06.066 (2006).
790 17 Aguilar, P. S., Hernandez-Arriaga, A. M., Cybulski, L. E., Erazo, A. C. & de Mendoza, D. Molecular
791 basis of thermosensing: a two-component signal transduction thermometer in Bacillus subtilis. *EMBO J*
792 **20**, 1681-1691, doi:10.1093/emboj/20.7.1681 (2001).
793 18 Halbleib, K. *et al.* Activation of the unfolded protein response by lipid bilayer stress. *Molecular cell* **67**,
794 673-684 e678, doi:10.1016/j.molcel.2017.06.012 (2017).
795 19 Cao, J., Schwichtenberg, K. A., Hanson, N. Q. & Tsai, M. Y. Incorporation and clearance of omega-3
796 fatty acids in erythrocyte membranes and plasma phospholipids. *Clinical chemistry* **52**, 2265-2272,
797 doi:10.1373/clinchem.2006.072322 (2006).
798 20 Oliveira, T. V., Maniero, F., Santos, M. H., Bydlowski, S. P. & Maranhao, R. C. Impact of high
799 cholesterol intake on tissue cholesterol content and lipid transfers to high-density lipoprotein. *Nutrition*
800 **27**, 713-718, doi:10.1016/j.nut.2010.07.018 (2011).
801 21 Gerl, M. J. *et al.* Quantitative analysis of the lipidomes of the influenza virus envelope and MDCK cell
802 apical membrane. *J Cell Biol* **196**, 213-221, doi:10.1083/jcb.201108175 (2012).
803 22 Sampaio, J. L. *et al.* Membrane lipidome of an epithelial cell line. *Proc Natl Acad Sci U S A* **108**, 1903-
804 1907, doi:1019267108 [pii]
805 10.1073/pnas.1019267108 (2011).
806 23 Levental, K. R. *et al.* Polyunsaturated lipids regulate membrane domain stability by tuning membrane
807 order. *Biophys J* **110(8)**, 1800-1810, doi:10.1016/j.bpj.2016.03.012 (2016).
808 24 Han, X. in *Lipidomics* 427-442 (John Wiley & Sons, Inc, 2016).
809 25 Klemm, R. W. *et al.* Segregation of sphingolipids and sterols during formation of secretory vesicles at the
810 trans-Golgi network. *J Cell Biol* **185**, 601-612, doi:jcb.200901145 [pii]
811 10.1083/jcb.200901145 (2009).

26 Ejsing, C. S. *et al.* Global analysis of the yeast lipidome by quantitative shotgun mass spectrometry. *Proc Natl Acad Sci U S A* **106**, 2136-2141, doi:0811700106 [pii] 10.1073/pnas.0811700106 (2009).
27 Sinensky, M. Defective regulation of cholesterol biosynthesis and plasma membrane fluidity in a Chinese hamster ovary cell mutant. *Proc Natl Acad Sci U S A* **75**, 1247-1249 (1978).
28 Sinensky, M. Adaptive alteration in phospholipid composition of plasma membranes from a somatic cell mutant defective in the regulation of cholesterol biosynthesis. *J Cell Biol* **85**, 166-169 (1980).
29 Dymond, M. K. Mammalian phospholipid homeostasis: homeoviscous adaptation deconstructed by lipidomic data driven modelling. *Chem Phys Lipids* **191**, 136-146, doi:10.1016/j.chemphyslip.2015.09.003 (2015).
30 Dymond, M. K., Hague, C. V., Postle, A. D. & Attard, G. S. An in vivo ratio control mechanism for phospholipid homeostasis: evidence from lipidomic studies. *J R Soc Interface* **10**, 20120854, doi:10.1098/rsif.2012.0854 (2013).
31 Sodt, A. J., Venable, R. M., Lyman, E. & Pastor, R. W. Nonadditive Compositional Curvature Energetics of Lipid Bilayers. *Phys Rev Lett* **117**, 138104, doi:10.1103/PhysRevLett.117.138104 (2016).
32 Almeida, P. F. Thermodynamics of lipid interactions in complex bilayers. *Biochim Biophys Acta* **1788**, 72-85, doi:10.1016/j.bbamem.2008.08.007 (2009).
33 Balogh, G. *et al.* Key role of lipids in heat stress management. *FEBS Lett* **587**, 1970-1980, doi:10.1016/j.febslet.2013.05.016 (2013).
34 Levental, K. R. *et al.* omega-3 polyunsaturated fatty acids direct differentiation of the membrane phenotype in mesenchymal stem cells to potentiate osteogenesis. *Science advances* **3**, eaao1193, doi:10.1126/sciadv.aao1193 (2017).
35 Psychogios, N. *et al.* The human serum metabolome. *PloS one* **6**, e16957, doi:10.1371/journal.pone.0016957 (2011).
36 Fan, Y. Y., McMurray, D. N., Ly, L. H. & Chapkin, R. S. Dietary (n-3) polyunsaturated fatty acids remodel mouse T-cell lipid rafts. *The Journal of nutrition* **133**, 1913-1920, doi:10.1093/jn/133.6.1913 (2003).
37 Stark, K. D. *et al.* Fatty acid compositions of serum phospholipids of postmenopausal women: a comparison between Greenland Inuit and Canadians before and after supplementation with fish oil. *Nutrition* **18**, 627-630 (2002).
38 Metcalf, R. G. *et al.* Effects of fish-oil supplementation on myocardial fatty acids in humans. *The American journal of clinical nutrition* **85**, 1222-1228 (2007).
39 van Blitterswijk, W. J., van der Meer, B. W. & Hilkmann, H. Quantitative contributions of cholesterol and the individual classes of phospholipids and their degree of fatty acyl (un)saturation to membrane fluidity measured by fluorescence polarization. *Biochemistry* **26**, 1746-1756 (1987).
40 Lande, M. B., Donovan, J. M. & Zeidel, M. L. The relationship between membrane fluidity and permeabilities to water, solutes, ammonia, and protons. *J Gen Physiol* **106**, 67-84 (1995).
41 Sessler, A. M., Kaur, N., Palta, J. P. & Ntambi, J. M. Regulation of stearoyl-CoA desaturase 1 mRNA stability by polyunsaturated fatty acids in 3T3-L1 adipocytes. *J Biol Chem* **271**, 29854-29858 (1996).
42 Levental, I. & Veatch, S. L. The continuing mystery of lipid rafts. *J. Mol. Biol.* **428**, 4749-4764 (2016).
43 Lin, X. *et al.* Domain stability in biomimetic membranes driven by lipid polyunsaturation. *J Phys Chem B* **120**, 11930-11941, doi:10.1021/acs.jpcb.6b06815 (2016).
44 Filippov, A., Oradd, G. & Lindblom, G. Domain formation in model membranes studied by pulsed-field gradient-NMR: the role of lipid polyunsaturation. *Biophys J* **93**, 3182-3190, doi:10.1529/biophysj.107.111534 (2007).
45 Budin, I. *et al.* Viscous control of cellular respiration by membrane lipid composition. *Science*, doi:10.1126/science.aat7925 (2018).
46 Brankatschk, M. *et al.* A Temperature-Dependent Switch in Feeding Preference Improves Drosophila Development and Survival in the Cold. *Dev Cell* **46**, 781-793 e784, doi:10.1016/j.devcel.2018.05.028 (2018).
47 Yeagle, P. L. Cholesterol and the cell membrane. *Biochim Biophys Acta* **822**, 267-287 (1985).
48 Crockett, E. Cholesterol Function in Plasma Membranes from Ectotherms: Membrane-Specific Roles in Adaptation to Temperature. *Integrative and Comparative Biology* **38**, 298-304 (1998).

865 49 Raghow, R., Yellaturu, C., Deng, X., Park, E. A. & Elam, M. B. SREBPs: the crossroads of physiological
866 and pathological lipid homeostasis. *Trends Endocrinol Metab* **19**, 65-73, doi:10.1016/j.tem.2007.10.009
867 (2008).
868 50 Sakai, J. *et al.* Molecular identification of the sterol-regulated luminal protease that cleaves SREBPs and
869 controls lipid composition of animal cells. *Molecular cell* **2**, 505-514 (1998).
870 51 Tang, J. J. *et al.* Inhibition of SREBP by a small molecule, betulin, improves hyperlipidemia and insulin
871 resistance and reduces atherosclerotic plaques. *Cell Metab* **13**, 44-56, doi:10.1016/j.cmet.2010.12.004
872 (2011).
873 52 Ye, J. & DeBose-Boyd, R. A. Regulation of cholesterol and fatty acid synthesis. *Cold Spring Harbor*
874 *perspectives in biology* **3**, doi:10.1101/cshperspect.a004754 (2011).
875 53 Kim, H. M. *et al.* A two-photon fluorescent probe for lipid raft imaging: C-laurdan. *Chembiochem* **8**, 553-
876 559, doi:10.1002/cbic.200700003 (2007).
877 54 Owen, D. M., Rentero, C., Magenau, A., Abu-Siniyeh, A. & Gaus, K. Quantitative imaging of membrane
878 lipid order in cells and organisms. *Nat Protoc* **7**, 24-35, doi:nprot.2011.419 [pii]
879 10.1038/nprot.2011.419 (2011).
880 55 Kaiser, H. J. *et al.* Order of lipid phases in model and plasma membranes. *Proc Natl Acad Sci U S A* **106**,
881 16645-16650, doi:0908987106 [pii]
882 10.1073/pnas.0908987106 (2009).
883 56 Gaus, K., Chklovskaia, E., Fazekas de St Groth, B., Jessup, W. & Harder, T. Condensation of the plasma
884 membrane at the site of T lymphocyte activation. *J Cell Biol* **171**, 121-131, doi:jcb.200505047 [pii]
885 10.1083/jcb.200505047 (2005).
886 57 Parasassi, T., De Stasio, G., Ravagnan, G., Rusch, R. M. & Gratton, E. Quantitation of lipid phases in
887 phospholipid vesicles by the generalized polarization of Laurdan fluorescence. *Biophys J* **60**, 179-189,
888 doi:10.1016/S0006-3495(91)82041-0 (1991).
889 58 Sezgin, E. *et al.* Adaptive lipid packing and bioactivity in membrane domains. *PloS one* **10**, e0123930,
890 doi:10.1371/journal.pone.0123930 (2015).
891 59 Levental, K. R. & Levental, I. Giant plasma membrane vesicles: models for understanding membrane
892 organization. *Current topics in membranes* **75**, 25-57, doi:10.1016/bs.ctm.2015.03.009 (2015).
893 60 Sezgin, E., Waithe, D., Bernardino de la Serna, J. & Eggeling, C. Spectral imaging to measure
894 heterogeneity in membrane lipid packing. *Chemphyschem* **16**, 1387-1394, doi:10.1002/cphc.201402794
895 (2015).
896 61 Feller, S. E., Gawrisch, K. & MacKerell, A. D., Jr. Polyunsaturated fatty acids in lipid bilayers: intrinsic
897 and environmental contributions to their unique physical properties. *J Am Chem Soc* **124**, 318-326 (2002).
898 62 Lorent, J. H. *et al.* The molecular and structural asymmetry of the plasma membrane. *bioRxiv*,
899 https://doi.org/10.1101/698837, doi:10.1101/698837 %J bioRxiv (2019).
900 63 Owen, D. M. *et al.* Fluorescence lifetime imaging provides enhanced contrast when imaging the phase-
901 sensitive dye di-4-ANEPPDHQ in model membranes and live cells. *Biophys J* **90**, L80-82,
902 doi:10.1529/biophysj.106.084673 (2006).
903 64 Venable, R. M., Kramer, A. & Pastor, R. W. Molecular Dynamics Simulations of Membrane
904 Permeability. *Chem Rev* **119**, 5954-5997, doi:10.1021/acs.chemrev.8b00486 (2019).
905 65 Manni, M. M. *et al.* Acyl chain asymmetry and polyunsaturation of brain phospholipids facilitate
906 membrane vesiculation without leakage. *eLife* **7**, doi:10.7554/eLife.34394 (2018).
907 66 Rotman, B. & Papermaster, B. W. Membrane properties of living mammalian cells as studied by
908 enzymatic hydrolysis of fluorogenic esters. *Proc Natl Acad Sci U S A* **55**, 134-141,
909 doi:10.1073/pnas.55.1.134 (1966).
910 67 Baron-Epel, O., Hernandez, D., Jiang, L. W., Meiners, S. & Schindler, M. Dynamic continuity of
911 cytoplasmic and membrane compartments between plant cells. *J Cell Biol* **106**, 715-721,
912 doi:10.1083/jcb.106.3.715 (1988).
913 68 Briolay, A., Jaafar, R., Nemoz, G. & Bessueille, L. Myogenic differentiation and lipid-raft composition of
914 L6 skeletal muscle cells are modulated by PUFAs. *Biochim Biophys Acta* **1828**, 602-613,
915 doi:10.1016/j.bbamem.2012.10.006 (2013).
916 69 Seo, J., Barhoumi, R., Johnson, A. E., Lupton, J. R. & Chapkin, R. S. Docosahexaenoic acid selectively
917 inhibits plasma membrane targeting of lipidated proteins. *FASEB journal : official publication of the*

Federation of American Societies for Experimental Biology **20**, 770-772, doi:10.1096/fj.05-4683fje (2006).

70 Yaqoob, P. *et al.* Comparison of the effects of a range of dietary lipids upon serum and tissue lipid composition in the rat. *The international journal of biochemistry & cell biology* **27**, 297-310 (1995).

71 Kusakabe, T. *et al.* Fatty acid synthase is expressed mainly in adult hormone-sensitive cells or cells with high lipid metabolism and in proliferating fetal cells. *J Histochem Cytochem* **48**, 613-622, doi:10.1177/002215540004800505 (2000).

72 Weiss, L. *et al.* Fatty-acid biosynthesis in man, a pathway of minor importance. Purification, optimal assay conditions, and organ distribution of fatty-acid synthase. *Biol Chem Hoppe Seyler* **367**, 905-912 (1986).

73 Murphy, E. J. Stable isotope methods for the in vivo measurement of lipogenesis and triglyceride metabolism. *J Anim Sci* **84 Suppl**, E94-104 (2006).

74 Nakagawa, Y., Sakumoto, N., Kaneko, Y. & Harashima, S. Mga2p is a putative sensor for low temperature and oxygen to induce OLE1 transcription in Saccharomyces cerevisiae. *Biochem Biophys Res Commun* **291**, 707-713, doi:10.1006/bbrc.2002.6507 (2002).

75 Tiku, P. E., Gracey, A. Y., Macartney, A. I., Beynon, R. J. & Cossins, A. R. Cold-induced expression of delta 9-desaturase in carp by transcriptional and posttranslational mechanisms. *Science* **271**, 815-818 (1996).

76 Burns, M., Wisser, K., Wu, J., Levental, I. & Veatch, S. L. Miscibility Transition Temperature Scales with Growth Temperature in a Zebrafish Cell Line. *Biophys J* **113**, 1212-1222, doi:10.1016/j.bpj.2017.04.052 (2017).

77 Eberle, D., Hegarty, B., Bossard, P., Ferre, P. & Foufelle, F. SREBP transcription factors: master regulators of lipid homeostasis. *Biochimie* **86**, 839-848, doi:10.1016/j.biochi.2004.09.018 (2004).

78 Yahagi, N. *et al.* A crucial role of sterol regulatory element-binding protein-1 in the regulation of lipogenic gene expression by polyunsaturated fatty acids. *J Biol Chem* **274**, 35840-35844 (1999).

79 Hannah, V. C., Ou, J., Luong, A., Goldstein, J. L. & Brown, M. S. Unsaturated fatty acids down-regulate srebp isoforms 1a and 1c by two mechanisms in HEK-293 cells. *J Biol Chem* **276**, 4365-4372, doi:10.1074/jbc.M007273200 (2001).

80 Xu, J., Teran-Garcia, M., Park, J. H., Nakamura, M. T. & Clarke, S. D. Polyunsaturated fatty acids suppress hepatic sterol regulatory element-binding protein-1 expression by accelerating transcript decay. *J Biol Chem* **276**, 9800-9807, doi:10.1074/jbc.M008973200 (2001).

81 Radanovic, T., Reinhard, J., Ballweg, S., Pesek, K. & Ernst, R. An Emerging Group of Membrane Property Sensors Controls the Physical State of Organellar Membranes to Maintain Their Identity. *BioEssays : news and reviews in molecular, cellular and developmental biology*, e1700250, doi:10.1002/bies.201700250 (2018).

82 Fan, Y. Y., Ly, L. H., Barhoumi, R., McMurray, D. N. & Chapkin, R. S. Dietary docosahexaenoic acid suppresses T cell protein kinase C theta lipid raft recruitment and IL-2 production. *J Immunol* **173**, 6151-6160 (2004).

83 Atkinson, T. G., Barker, H. J. & Meckling-Gill, K. A. Incorporation of long-chain n-3 fatty acids in tissues and enhanced bone marrow cellularity with docosahexaenoic acid feeding in post-weanling Fischer 344 rats. *Lipids* **32**, 293-302, doi:10.1007/s11745-997-0036-x (1997).

84 Owen, A. J., Peter-Przyborowska, B. A., Hoy, A. J. & McLennan, P. L. Dietary fish oil dose- and time-response effects on cardiac phospholipid fatty acid composition. *Lipids* **39**, 955-961, doi:10.1007/s11745-004-1317-0 (2004).

85 Rawson, R. B., DeBose-Boyd, R., Goldstein, J. L. & Brown, M. S. Failure to cleave sterol regulatory element-binding proteins (SREBPs) causes cholesterol auxotrophy in Chinese hamster ovary cells with genetic absence of SREBP cleavage-activating protein. *Journal of Biological Chemistry* **274**, 28549-28556 (1999).

86 Pirro, M. *et al.* Plasma free fatty acid levels and the risk of ischemic heart disease in men: prospective results from the Quebec Cardiovascular Study. *Atherosclerosis* **160**, 377-384 (2002).

87 Tulodziecka, K. *et al.* Remodeling of the postsynaptic plasma membrane during neural development. *Mol Biol Cell* **27**, 3480-3489, doi:10.1091/mbc.E16-06-0420 (2016).

970 88 Surma, M. A. *et al.* An automated shotgun lipidomics platform for high throughput, comprehensive, and
971 quantitative analysis of blood plasma intact lipids. *European journal of lipid science and technology :*
972 *EJLST* **117**, 1540-1549, doi:10.1002/ejlt.201500145 (2015).
973 89 Liebisch, G. *et al.* High throughput quantification of cholesterol and cholesteryl ester by electrospray
974 ionization tandem mass spectrometry (ESI-MS/MS). *Biochim Biophys Acta* **1761**, 121-128,
975 doi:10.1016/j.bbalip.2005.12.007 (2006).
976 90 Sezgin, E. *et al.* Elucidating membrane structure and protein behavior using giant plasma membrane
977 vesicles. *Nat Protoc* **7**, 1042-1051, doi:10.1038/nprot.2012.059 (2012).
978 91 Levental, K. R. & Levental, I. Isolation of giant plasma membrane vesicles for evaluation of plasma
979 membrane structure and protein partitioning. *Methods in molecular biology* **1232**, 65-77,
980 doi:10.1007/978-1-4939-1752-5_6 (2015).
981